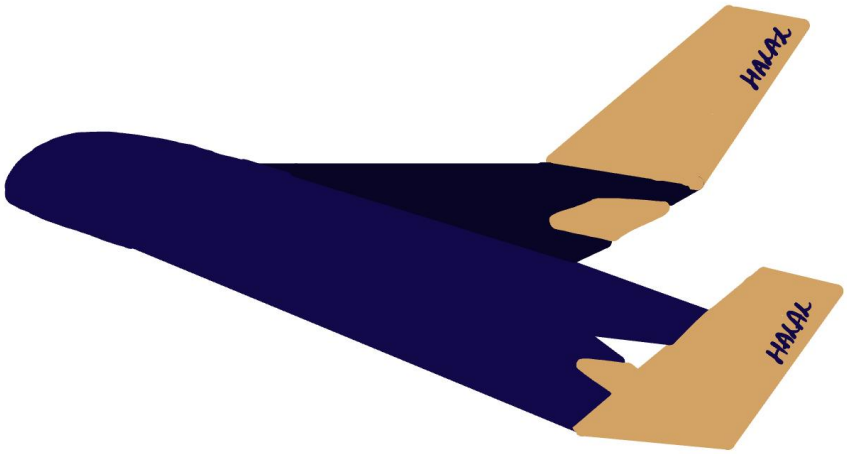

AER406 Aircraft Design

Final Design Report

Team One (Halal BWB)

Aidan Grenville (1004894206)
Elif Çelik (1004027607)
Hyungin (Fred) Chun (1004924834)
Prachi Sukhnani (1005065812)

Table of Contents

A. Introduction

Team BWB is pleased to present ***Halal 2023***, a Blended Wing Body (BWB) aircraft designed to carry tennis, golf, and ping pong balls around a circuit. *Halal 2023* is powered by an electric motor and propeller, and is controlled with an onboard computer in addition to ground-based pilot inputs. *Halal 2023* will takeoff from a short asphalt runway and fly its payload around a circular course, earning points through the design's stability, endurance, STOL performance, and most importantly, payload capacity. A highly swept wing with a large root chord is a characteristic feature of *Halal 2023*, tapering away to a reflexed wingtip. The fuselage portion, in standard BWB fashion, also functions as an airfoil, and contains the majority of payload and avionics.

A1. Mission Analysis

The objective of this mission is to design, build and fly a radio-controlled blended wing body aircraft, with the goal of scoring the highest possible points using a prescribed cost function, as explained in the next section. Three different flight courses are to be considered for this mission. For each of the missions, two markers that are 100 meters apart will be used, as shown in Figure I.1.

Figure I.1: Mission Setup [A1]

1. Initial Flight

   Aircraft will complete 1 lap with no payload to prove that it is safe to fly before proceeding to the scoring flights.

2. Efficiency Flight Course

   3 laps of course will be flown using Pixhawk, and aircraft is to maintain a level flight attitude when it passes each marker. The energy used to fly 3 laps (6 straight segments and 5 turns) in Joules will be calculated as 1/E.

3. Field Stability Course

   Lastly, the distance the aircraft can fly without needing a control input will be determined. The higher this distance, the higher the flight stability course score will be.

A2. Cost Function

The cost function or “flight score” for this design challenge is as follows:

$$FS = CU^{0.8} \times \left(\frac{3200}{E}\right)^2 \times \min(PF,\, 0.25) \times TB \times CB \times STB$$

Table 1 describes each term and how they will be optimized to maximize the flight score:

Table A.1: Cost Function Terms & Optimization Plans

Term	Meaning	Value
CU	Cargo Units	560 cargo units (4 tennis balls, 2 golf balls, 6 ping pong balls)
$\left(\frac{3200}{E}\right)^2$	Energy	Energy measured as the Joules required to fly 3 laps is 2488 W.
$\min(PF,\, 0.25)$	Payload Fraction	For the ratio of payload mass to aircraft mass (payload + empty weight), min(0.27, 0.25) is used
TB	Take-off Bonus	Aircraft that takeoff in 25 feet receive a multiplier of 1.25. Else, TB = 1. Since the takeoff distance is less than 25 feet as outlined in the Performance section of this report, this term is 1.25.
CB	Configuration Bonus	1.5 for Blended Wing Body
STB	STB = 1 + 0.2D* where D* is the fraction of the 100m traveled with pilot input	1 is used to be conservative

Using Table A.1, the expected score is approximately **127**.

A3. Requirements

A list of design requirements and constraints have been gathered in Table A.2. This comprehensive list was created considering the requirements of the design problem and the optimization plans outlined in Table A.1 for the cost function.

Table A.2: System Requirements & Constraints

ID	Requirement	Justification
1	Aircraft take-off distance	The cost function as shown above is dependent on the value of the take-off bonus. Since the objective is to maximize the flight score, the maximum possible TB value of 1.25 is to be achieved. This is possible when the aircraft

		takes off within 25 feet [A1, Slide 20]. In order to decrease the take-off distance, the lift required that will be generated by the flaps will be considered an important design decision. Thus, the takeoff distance shall be at most 25 feet.
2	Cargo Units	The cargo units selected must be between 100 - 800 when determining the cost function, as defined by the design problem [A1, Slide 21]. For our design, 460 cargo units will be used in the calculation of the cost function. Thus, at most 460 cargo units shall be carried onboard. This is the maximum possible cargo units available based on a tradeoff conducted (shown in Appendix A.1)
3	Cargo Positioning	Weight distribution inside the aircraft is crucial to maintain the same center of gravity (COG). If the cargo distribution changes, the COG might shift aft of its allowable limit, causing instability [A2]. Thus, the CG, located at approximately 32 cm along the chord of the fuselage, shall always be ahead of the neutral point.
4	Trade-off Between Flight Performance & Cost Function	When the weight of an aircraft is too high, the performance of the flight is impacted in a negative way. An excessive weight may require a longer take-off run, a reduced angle of climb and reduced maneuverability. Increasing the weight of the payload increases the cost function score. Thus, when the cargo units are being selected, the challenges associated with the flight performance of an aircraft with a high weight should be taken into account [A2]. Thus, at most 321.3g of cargo mass will be carried onboard (7 golf balls). This is the maximum possible mass based on the payloads available (shown in Appendix A.1)
5	Attachment of Battery	The battery shall be loaded/removed easily for testing and construction purposes [A3].
6	Attachment of Cargo	The cargo shall be loaded/removed easily to allow for testing of different weights in the case that the aircraft shows unexpected behaviour and adverse performance [A3].
7	Attachment of Motor	The motor might oscillate if it is not balanced. If it oscillates at the right frequency, the oscillation might transfer onto the wings of the aircraft, possibly leading to flutter and destruction of the wings [A4]. Thus, the motor shall be fastened securely onto a stiff surface.
8	Propulsive efficiency	Since the cost function is inversely related to the square of the energy, the energy used should be minimized to maximize the flight score. This is possible through ensuring that the propulsive efficiency for the first estimate is at least 50% [A1, Slide 13].
9	Positioning of	The equipment such as the GPS, Spektrum, receiver, telemetry antenna shall be

	the Equipment	located away from motors to avoid interference [A4].
10	Minimum Airspeed	As defined in the design problem, the minimum airspeed must be 10 m/s [A1, Slide 13].
11	Payload Fraction	The cost function is dependent on the payload fraction of the aircraft. To maximize the min(PF, 0.25) term in the cost function, PF should be as close to 0.25 as possible [A1, Slide 18].
12	Positive Stability Control	The aircraft must be able to return to the desired trajectory after the occurrence of unexpected perturbations, to allow for stable flight [A6].

A4. Design Summary Table

Table A.3 provides a conclusive summary of Halal BWB's design.

Table A.3: Design Summary

Wing	
Area (S)	0.403 m^2
Reference Area (S_{ref})	0.52 m^2
Aspect Ratio (AR)	3.875
Span (b)	1.424 m
Taper Ratio (λ)	0.3
Root Chord (c_{root})	0.563 m
Tip Chord (c_{tip})	0.169 m
Mean Aerodynamic Chord (MAC)	0.297 m
Sweep (Λ)	35°
Twist	-5°
Dihedral	0°
Wetted Area (S_{wet})	0.825 m^2

Airfoil	MH 60
Vertical and Horizontal Surfaces (Winglets)	
Area (S)	0.025 m^2
Span (b)	0.2 m
Taper Ratio (λ)	0.5
Tip Chord (c_{tip})	0.085 m
Root Chord (c_{root})	0.169 m
Sweep (Λ)	35°
Dihedral	90°/Vertical
Wetted Area (S_{wet})	0.050 m^2
Airfoil	Rectangle/Flat Plate
Fuselage	
Length	0.818 m
Max Thickness	0.118 m
Wetted Area (S_{wet})	0.039 m^2
Airfoil	MH 78
Geometry, Relative to Fixed Location	
NP Location(s), Including Method Used to Determine	Cruise Conditions, Full Payload: 0.367 m Cruise Conditions, No Payload: 0.367 m Takeoff Conditions, Full Payload: 0.354 m Takeoff Conditions, No Payload: 0.394 m + XFLR5 Direct Analysis
CG Locations for Different Loads	Full Payload: 0.3236 m No Payload: 0.334 m
Wing and Tails ¼ Chord Locations (For Swept at Centerline of Fuselage)	Wing ¼ Chord Location: 0.204 m
Performance	

$C_{D,0}$ + Method Used to Estimate and What Was Included (i.e. Variable Re, Propwash, . . .)	0.028 + Drag Build-up Method + Wings, Fuselage, Landing Gears
e, Plus Method Used to Estimate	0.791 + Shevell Method
Estimated TO Length(s)	6.09 - 7.65 m Flat, level, dry turf runway. Headwinds from 1.5 to 0.5 m/s Ground, slipstream, and wind effects considered.
Cruise Speed and Energy Usage	10.5 m/s design cruise speed (level, accelerated) 2490 W for indicative efficiency course (3 laps) Sum of power used from thrust required for level flight and that required for 25° bank.
Stall Speed	7.65 m/s
Weights	
Total/Payload/Empty Weights for Different Loading Conditions	M_{TO} = 1.33 kg $M_{Landing}$ = 1.33 kg M_{Empty} = 0.97 kg
Final Weight Fractions PF, W_e/W_0	PF = 0.27 W_e/W_0 = 0.73
Inertia Estimates for Different Loading Conditions	I_{XX} = 0.030 kgm^2 I_{YY} = 0.031 kgm^2 I_{ZZ} = 0.062 kgm^2 I_{XZ} = 0.000 kgm^2
Structures	
Maximum Design Load Factor	n = 3.6 *Full down control deflection for minimum pull down radius, maneuvering speed*
Maximum Maneuvering Speed	16.0 m/s
Minimum Resulting SF for Spar and Other Main Components Analyzed, Indicate Type of Analysis (i.e. Bending, Bearing, Buckling, etc . . .)	1.1 This tops up to a n ≈ 4 from the already aggressive dive load factor calculated above.
Maximum Deflection of Spar at Maximum Design Load Factor	0.018 m
Stability/Control	

Static Margin at Different Load/Speed Conditions	Cruise Conditions, Full Payload: 15 % Cruise Conditions, No Payload: 11 % Takeoff Conditions, Full Payload: 10 % Takeoff Conditions, No Payload: 20 %
Static Trim Control Deflections at Take-Off and Cruise Conditions for Different Loads	Cruise Conditions, Full Payload: -1.5° Cruise Conditions, No Payload: 1° Takeoff Conditions, Full Payload: -2.5° Takeoff Conditions, No Payload: -1°
$C_{m,\alpha}$ at Different Loads/Speeds	Cruise Conditions, Full Payload: -0.00334/° Cruise Conditions, No Payload: -0.00369/° Takeoff Conditions, Full Payload: -0.00311/° Takeoff Conditions, No Payload: -0.00353/°
Eigenvalues, Time to Double/Half, Damping Ratio for Dynamic Stability Modes at Different Loads/Speeds (At Least Take-Off + Cruise)	**Cruise, Full Payload** - **Short Period:** Eigenvalues: $-10 \pm 9.187i$, undamped frequency: $13.58\ rad/s$, time to double/half: 0.0693s, damping: 0.74 - **Phugoid:** Eigenvalues: $0.002236 \pm 1.053i$, undamped frequency: 1.053 rad/s, time to double/half: 309.9s, damping: -0.0021 - **Roll**: Eigenvalues: -36.93, to double/half:0.019s - **Dutch Roll:** Eigenvalues: $-1.315 \pm -7.13i$, undamped frequency: $7.25\ rad/s$, time to double/half: 0.526s, damping: 0.18 - **Spiral:** Eigenvalues: 0.1093, to double/half: 6.3s **Takeoff, Full Payload** - **Short Period:** Eigenvalues: - $-7.717 \pm 6.354i$, undamped frequency: $9.99\ rad/s$, time to double/half: 0.089s, damping:0.772 - **Phugoid:** Eigenvalues: $-0.005353 \pm 1.193i$, undamped frequency: 1.19 rad/s, time to double/half: 129.4s, damping:0.0045 - **Roll**: Eigenvalues: -27.94, to double/half:0.0248s - **Dutch Roll:** Eigenvalues: $-1.535 \pm -6.978i$, undamped frequency: $7.14\ rad/s$, time to double/half: 0.451 s, damping: 0.215 - **Spiral:** Eigenvalues: 0.1694, to double/half: 4.1s
Chord and Span for Control Surfaces and Location Along Wing for Elevons/Ailerons	Mean Chord: 0.075 m Span: 0.24 m Location Along Wing: 40% (0.24 m - 0.48m) Elevon Chord to Wing Chord: 25% Control Surface Area: 0.018 m^2

Maximum Hinge Moment Torques and Associated Flight Conditions	Cruise, Full Payload Hinge Moment: 8.38E-6 N m Takeoff, Full Payload Hinge Moment: 4.46E-5 N m Turn, Full Payload Hinge Moment: 1.05E-5 N m

B. Aerodynamics

B1. Airfoils

For the main wing, the MH 60 airfoil was selected, as shown in Figure B.1. This airfoil was designed by Martin Hepperle specifically for tailless model flying wings, and have shown to be successful in the past. It has a thickness-to-chord ratio of 10.12%, and it can be used at Reynolds numbers of 150 000 and above. Our expected Reynolds number at cruise conditions is 203 368 at the reference chord (mean aerodynamic chord of our reference wing, which is 0.297 m), thus this airfoil is appropriate for the wings of our aircraft. Its $c_{m,c/4}$ is a low positive value of + 0.0140.

For the fuselage, the MH 78 airfoil was chosen, as shown in Figure B.2. This airfoil has a thickness-to-chord ratio of 14.4%, and this high maximum thickness value was the main driving factor of our airfoil selection, as sufficient cargo space is needed.

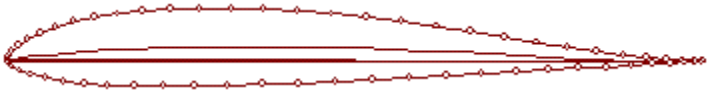

Figure B.1: MH 60 Airfoil.

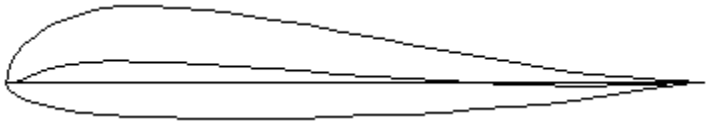

Figure B.2: MH 78 Airfoil.

A flat plate is used for the winglets instead of a streamlined geometry as its thickness is too small to be manufactured accurately with an airfoil cross-section.

B2. Configuration

Our aircraft consists of a blended-wing body configuration. The leading edges of the wings are offset from the leading edge of the fuselage by 0.079 m. Winglets were added to the tips of the wings to reduce induced drag and to improve lateral stability. The wings are twisted by -5° in combination with the reflexed MH 60 airfoil of the wings in order to improve the longitudinal static stability of the aircraft. We did not find a reason to change the dihedral of the wings, thus the dihedral angle is left as 0°.

B3. Planform

Our aspect ratio (AR) was assumed to be 3.875 from historical data. The reference wing area (S_{ref}) was calculated to be 0.52 m^2 from our limiting wing loading value. The span length (b) was then calculated to

be 1.424 m. A taper ratio (λ) of 0.3 was chosen, as this is where the lowest induced drag factor occurs for an AR value of approximately 4. Thus, our root and tip chords (c_{root} and c_{tip}) of our trapezoidal reference wing area are 0.563 m and 0.169 m, respectively. Our mean aerodynamic chord (MAC) was then calculated to be 0.297 m. Our wings also have a sweep angle (Λ) of 35° about the quarter chord for improving the longitudinal static stability for tailless aircraft such as ours. The actual or exposed area of the wings were calculated to be 0.403 m^2. The wetted area (S_{wet}) of the wings was approximated to be 0.825 m^2.

The chord length of our fuselage ($c_{fuselage}$) is 0.818 m. The wetted area (S_{wet}) of the fuselage was approximated to be 0.039 m^2.

For the winglets, the root chord (c_{root}) is constrained to be the same as the tip chord of the wings, which is 0.169 m as mentioned above. Its span (b) or height was decided to be 0.2 m, based on the fact that it had to be longer than the root chord of the winglets (from Raymer). A taper ratio (λ) of 0.5 was chosen to set the tip chord (c_{tip}) to be 0.084 m, which enables the thickness to be 6 mm for our thickness-to-chord ratio of 8%. Anything smaller in thickness would make it difficult for construction. The winglets are vertical, i.e. the winglets have a dihedral angle of 90°.

B4. Lift Distributions

The spanwise lift distributions for various flight configurations are shown in Figures B.3, B.4, B.5, and B.6 below. The exact trim conditions are explained in greater detail in the stability sections.

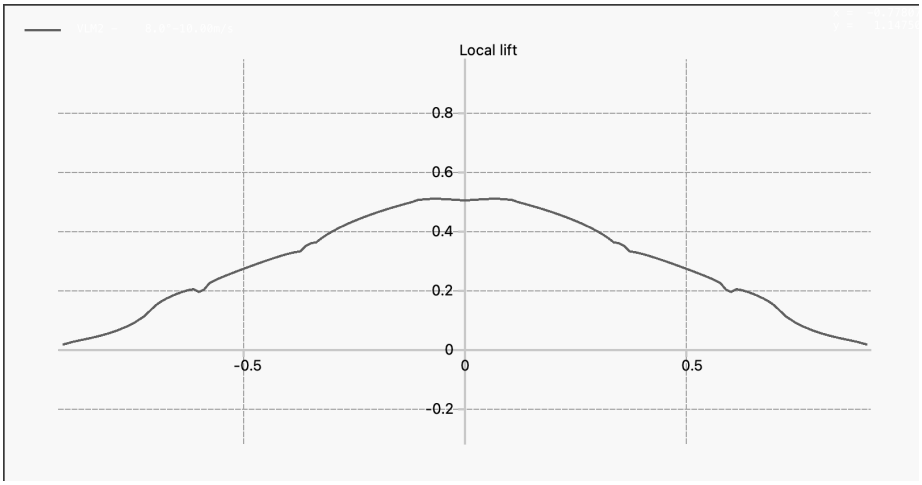

Figure B.3: Spanwise Lift Distribution at Cruise Conditions With Full Payload.

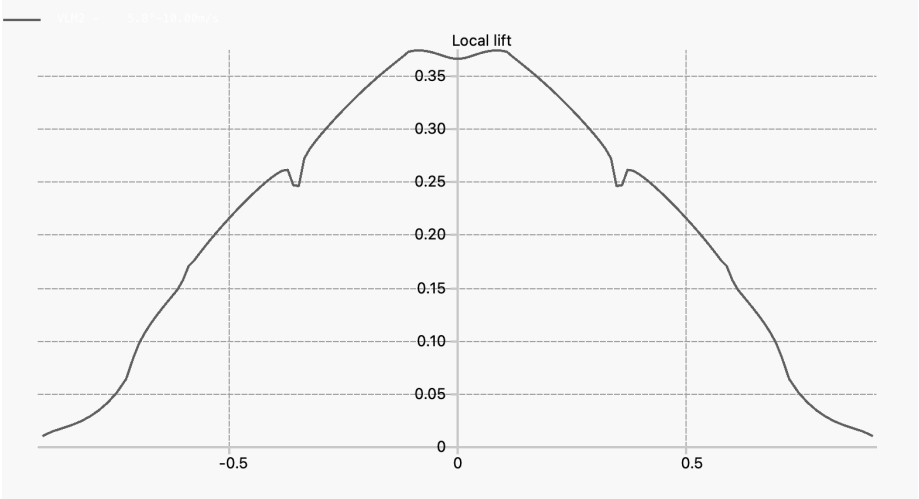

Figure B.4: Spanwise Lift Distribution at Cruise Conditions With No Payload.

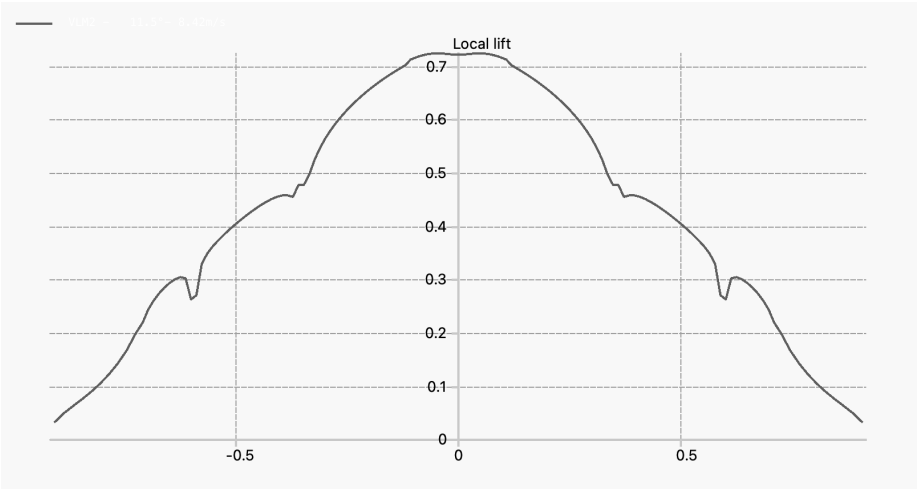

Figure B.5: Spanwise Lift Distribution at Takeoff Conditions With Full Payload.

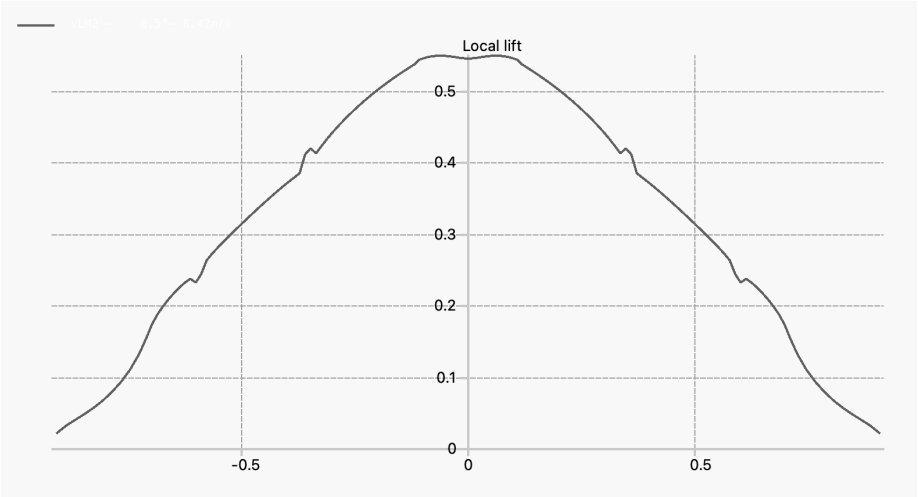

Figure B.6: Spanwise Lift Distribution at Takeoff Conditions With No Payload.

B5. C_l Distributions

The spanwise coefficient of lift distributions for various flight conditions are shown in Figures B.7, B.8, B.9, and B.10 below. The exact trim conditions are explained in greater detail in the stability sections.

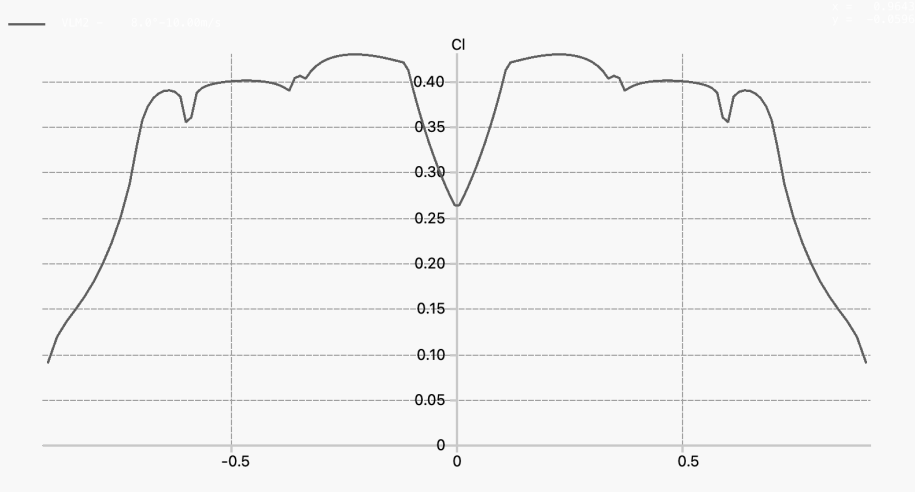

Figure B.7: Spanwise C_l Distribution at Cruise Conditions With Full Payload.

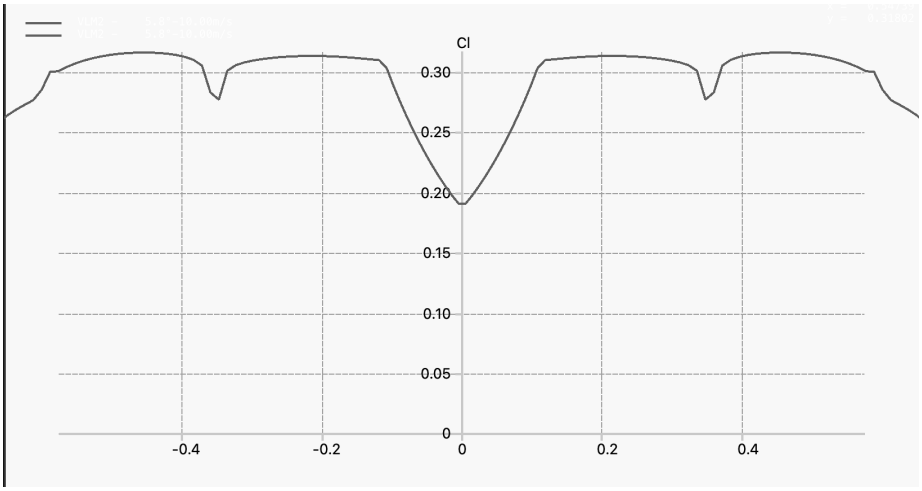

Figure B.8: Spanwise C_l Distribution at Cruise Conditions With No Payload.

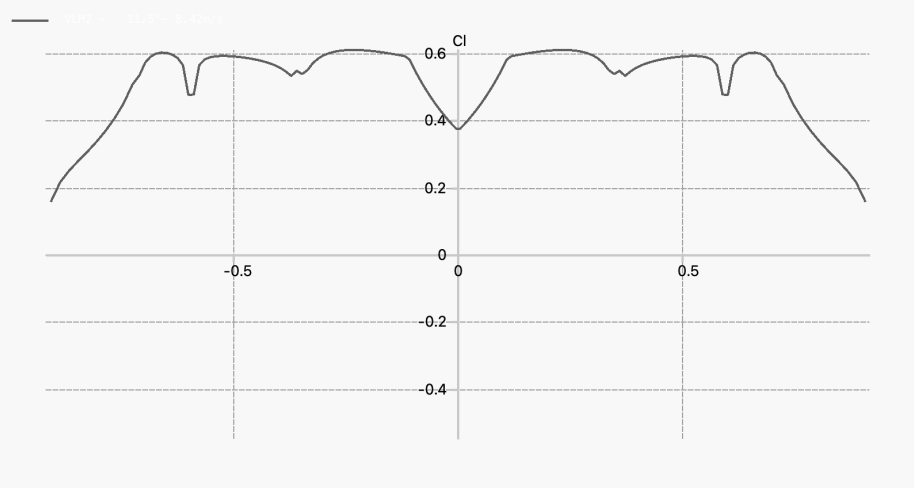

Figure B.9: Spanwise C_l Distribution at Takeoff Conditions With Full Payload.

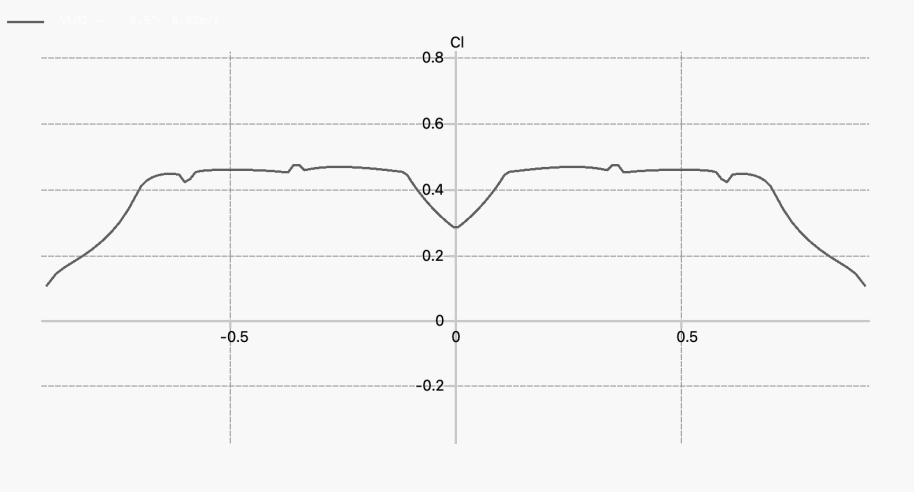

Figure B.10: Spanwise C_l Distribution at Takeoff Conditions With No Payload.

B6. C_l Max Values

The $c_{l,max}$ of the wing airfoil (MH 60) is given as 1.15 at α of 12° and Reynolds number of 200 000, while the $c_{l,max}$ of the fuselage airfoil (MH 78) is given as 1.25 at α of 12° and Reynolds number of 200 000, as shown in Figure B.11.

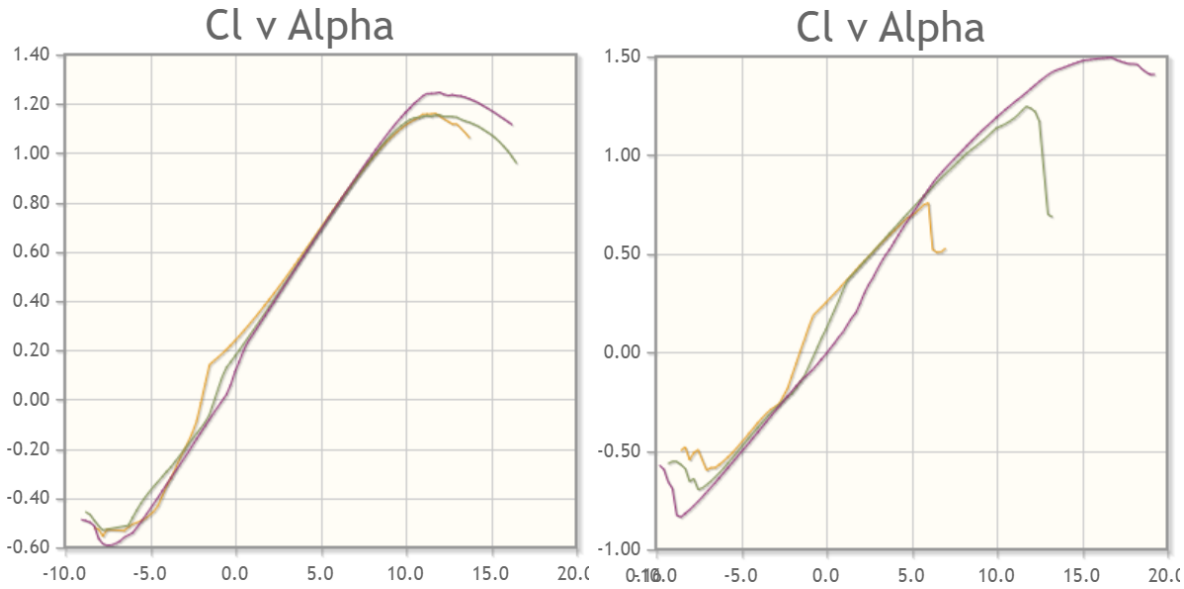

Figure B.11: Lift Curve Slopes for the MH 60 Airfoil (Left) and the MH 78 Airfoil (Right) for Reynolds Numbers of 100 000 (Orange), 200 000 (Green), and 500 000 (Purple) Adapted From Airfoil Tools.

B7. C_L Max Value

Our $C_{L,max}$ is uncertain, as XFLR5 crashed when we conducted direct analysis for angles of attack greater than 15°. For cruise conditions with full payload at α of 15°, C_L is given as approximately 0.8, which we assume to be our $C_{L,max}$.

B8. Zero-Lift Drag Coefficient

The zero-lift drag coefficient, or the parasite drag coefficient at zero lift, can be estimated for an entire aircraft by adding together the estimates for each major component *i* (fuselage, wing, tails, etc.):

$$C_{D,0} = \sum_i k_i c_{f,i} \frac{S_{wet,i}}{S_{ref}} Q_i$$

where k_i is the form factor, $c_{f,i}$ is the skin friction coefficient, $S_{wet,i}$ is the wetted area, S_{ref} is the reference area, and Q_i is the interference effect when components are brought together. The full wing area of 0.52 m^2 is used as S_{ref}. Table B.1 below summarizes the parameters and the zero-lift drag coefficients calculated for the wing and fuselage.

Table B.1: Zero-lift Drag Coefficients for the Wing and Fuselage.

Component (*i*)	**Form Factor (k_i)**	**Skin Friction Coefficient ($c_{f,i}$)**	**Wetted Area (S_{wet}) [m^2]**	**Interference Effect (Q_i)**	**Zero-Lift Drag Coefficient ($C_{D,0}$)**
Wing	2.637	3.579E-3	0.825	1.0	0.0150
Fuselage	2.637	1.774E-3	0.339	1.0	0.0030

To estimate the $C_{D,0}$ of the landing gears, the width of the tires were approximated to be ⅓ of the tire diameters. The length of each landing gear wire was approximated to be 0.065 m for sufficient propeller clearance. Ultimately, the $C_{D,0}$ of the landing gears was calculated to be 0.007389. Summing the $C_{D,0}$ of the individual components and multiplying by a fudge factor of 1.1 (smaller than the larger fudge factor of 1.3 used previously), the $C_{D,0}$ of the aircraft is 0.028, which is lower than the value calculated previously (using the equation in Raymer, page 328).

B9. Oswald Efficiency Factor

The Oswald efficiency factor *e* can be found as: $e = \frac{1}{\frac{1}{e_{inviscid}} + \pi(AR)KC_{D,0}}$

where $e_{inviscid}$ is the span efficiency factor, *AR* is the aspect ratio of the wing, *K* is the sweep factor, and $C_{D,0}$ is the zero-lift drag coefficient found above. A value of 0.9 was chosen for $e_{inviscid}$, as the wing of our aircraft is swept and twisted. *K* was approximated to be 0.45 for our sweep angle of 35°. Consequently, the Oswald efficiency factor *e* was updated to be 0.791, which is reasonable as typical values for *e* are between 0.7 and 0.9.

From direct analysis in XFLR5, an “efficiency” of 0.613 was given at cruise conditions with full payload. It is unclear whether this value is the inviscid span efficiency factor or the Oswald efficiency factor. In any case, it is much lower than what we expect compared with historical data, and thus it is dismissed to be inaccurate.

C. Structural

Figure C.1 and C.2 present an isometric view and an engineering drawing for the HALAL 2023 BWB. All dimensions in Figure C.2 are in meters. The structure consists of 1 fuselage and 2 wings. All three sections of the aircraft are shaped as airfoils to increase lift. Furthermore, the relative chord lengths and positions of the airfoils have been selected to classify the aircraft as a BWB. This section of the report will cover the external and internal structural design of the BWB, concluding with material selection and a build plan.

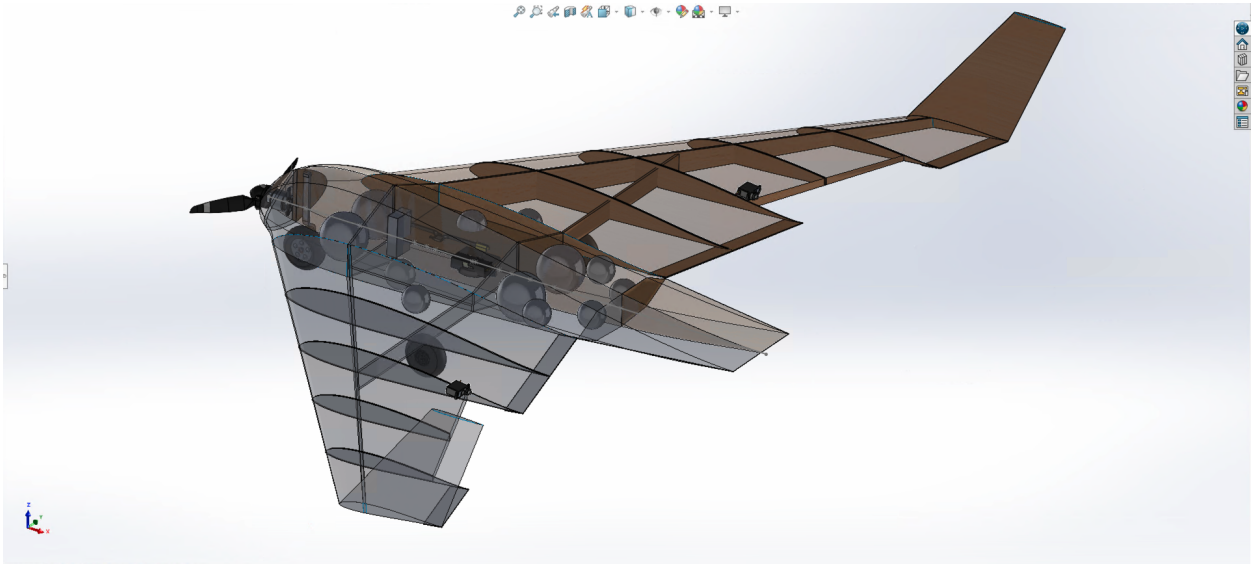

Figure C.1 *HALAL 2023 Isometric View*

C1. External Design

The fuselage consists of the MH78 and MH60 airfoils (for the center and edges of the fuselage respectively). The MH60 airfoil is also the root of the wing. The nose of the fuselage is curved to allow for a seamless transition to the wing while allowing for ample room at the front for the thrust box and firewall. The hollow area of the fuselage is cut off at the trailing edge of the wing. Beyond this point, the fuselage “tail” is treated as a solid shape and contains no components. This is due to the fact that there is little vertical clearance to place components, and accessing this area without an additional hatch will not be possible. This tail, which doesn’t pose any aerodynamic consequences from its design, is trapezoidal in shape to keep construction simple.

The wing blends directly into the fuselage of the BWB, starting with the MH60 airfoil, and tapering off to an MH64 airfoil at a -5˚ twist to improve longitudinal stability. The wing is also swept back at approximately 35˚ at the quarter-chord. Furthermore, to improve stability, an elevon has been added to each wing, spanning ⅝ of the length of each wing, and consuming about a quarter of the chord of the wing at the relevant points. These elevons are trapezoidal in shape, and taper to a point to keep the elevons streamlined with the overall wing. The elevons will be controlled with a servo motor placed close to the inner corner of the elevon, via a linear actuator attached to the motor. Note that an inner wing or transition

wing was considered during the conceptual design phase, but due to an increased complexity of manufacturing, it was ruled out.

Lastly, winglets have been added to the design to reduce drag and improve lateral stability. While the CAD model shows an airfoil at the winglet tip, the real-life winglet will be a simple trapezoidal sheet. The winglet is also swept back at 35˚ from the quarter chord of the wing tip. The winglet is about 0.2m in height and will be perpendicular to the plane of the wing.

C2. Internal Design

Figure C.3 shows a bird's eye view of the HALAL BWB, with all internal support structures and approximate avionics and payload locations. This section will cover the internal design in detail, and the following section will cover the layout.

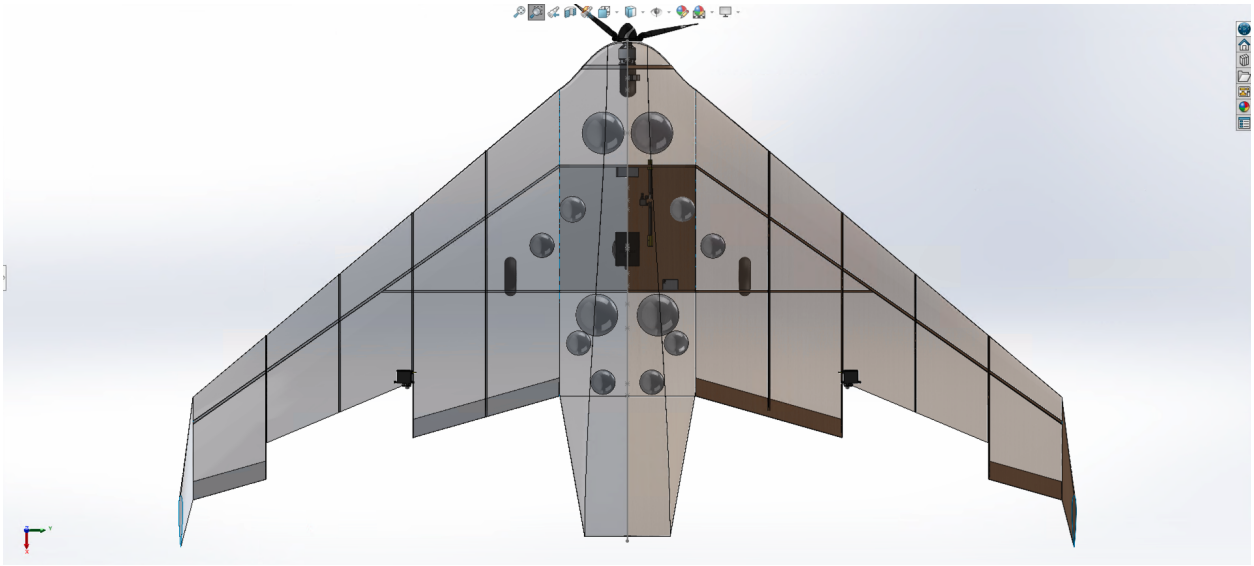

Figure C.3 *HALAL 2023 Internal Design & Layout*

The fuselage (not including the tail), is split into 3 sectors, split up by the main spar and the secondary spar. The main spar, located at the quarter chord of the wing, joins the main spars in the wings together across the fuselage—this interface which will be discussed below. The secondary spar is located halfway along the fuselage chord, and extends into the wings, meeting the main spar. The sections of these spars within the fuselage are roughly trapezoidal to simplify manufacturing while maximizing the amount of support provided to the fuselage. Note that sector 2, where the Pixhawk is located, is supported by a floor along the Z = 0 plane so that the Pixhawk can be as close to the center of gravity of the plane as possible. The floor will also support the secondary landing gear. A similar floor may be added to the first sector to support the nose gear. Two hatches are slated to allow access to all 3 sectors, as shown in Figure C.4. These hatches will be placed approximately over the 2 support spars, but the exact design is to be determined. The hatches will open against the streamline as needed, which ensures the hatch will stay closed due to oncoming wind during flight.

The wing's internal support structure, as shown in Figure C.5, consists of 1 main spar along the quarter-chord, and 6 ribs (4 internal + 2 end caps). There is a trailing edge present where there is no elevon, and not visualized is a thin leading edge spar. Spar sizing is shown in Appendix C.1, where it was determined that a simple 3mm rectangular beam would be sufficient to support loading across the wing. Following the guidance that ribs should be ~10 cm apart, the 4 ribs in the wing are 12 cm apart. Once again, 3mm thick balsa was the material of choice. Rib 4 is cut off due to the elevon placement.

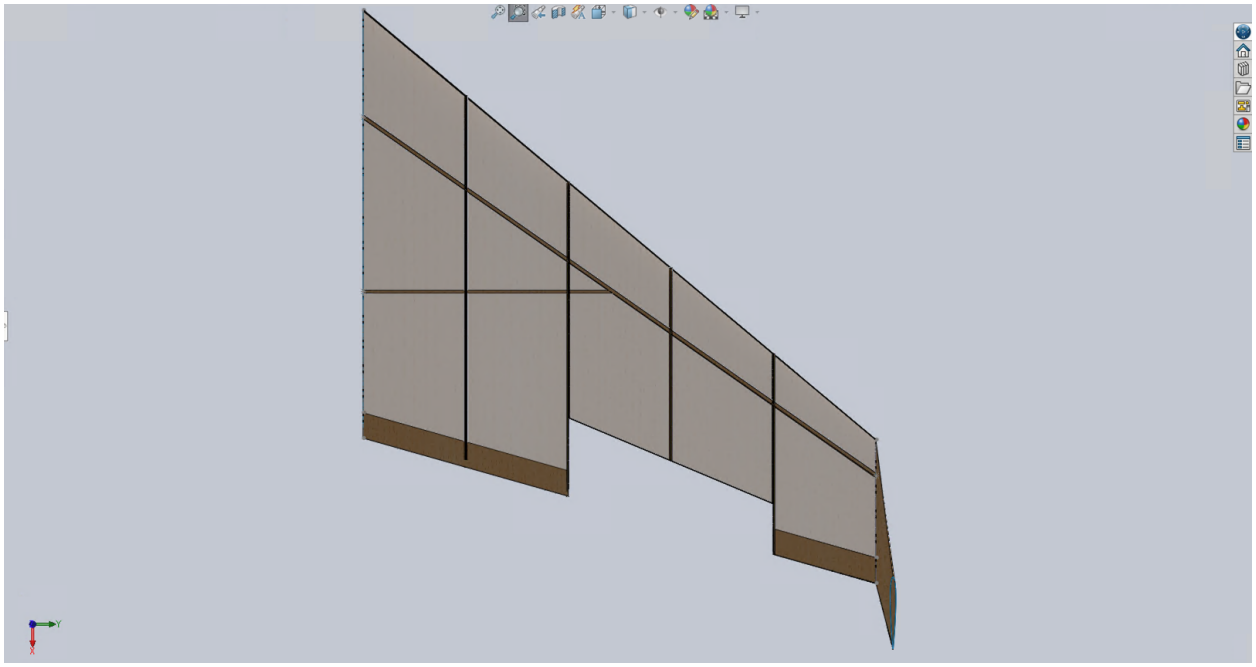

Figure C.5 *Wing Support Structure*

C3. Internal Layout

Table C.1: Design Rationale for Layout

Consideration	**Explanation**
1: *Functionality*	If equipment 'must' be placed in a certain location as a design critical consideration, then this factor has to be considered first.
2: *Accessibility*	Much of our equipment needs to be accessible to an operator pre- or post-flight. Equipment needs to be accessible through a hatch for repairs.
3: *Symmetry*	To minimize the necessity of trimming to avoid roll in steady, level flight, equipment should be on the centerline or mirrored around the centerline.
4: *Simplicity*	Wire runs, build difficulty, and mounting feasibility all contribute to simplicity, which is examined, but does not trump other considerations.

Table C.2 summarizes the components that are placed within each sector of the fuselage.

Table C.2: Layout Overview by Sector

Sector	Payloads	Avionics
1	2 x Tennis Balls	1 x Thrust Box + Firewall] 1 x ESC 1 x Landing Gear 1
2	2 x Golf Balls 2 x Ping Pong Balls (Placed in wing adjacent to sector 2)	1 x Battery 1 x Battery Management Chip 1 x Transmitter + Antenna 1 x Receiver 1 x Pixhawk 1 x GPS 1 x Landing Gear 2
3	2 x Tennis Balls 4 x Ping Pong Balls	-

Not placed within a particular sector are the servos—they are largely located outside the plane at the inner corner of the elevons, while the wiring will be directed through the wing into the fuselage.

Table C.3 gives the exact X and Y-axis stations of most components, and a subsequent CoG estimate.

Table C.3: Location Stations, CoG Estimate and Mass Properties

Table C.3.1: Location Stations

Class	Element	X-Station (cm)	Mass(g)
Avionics	Pixhawk	34	38
	GPS/Compass	34	32
	Power Module	26	22
	Turingy Motor	2.6	67
	Propeller	0	25
	ESC	5	36
	RPM Sensor	2.5	5
	Radio Receiver	40	6
	Servo 1	56	12
	Servo 2	56	12
	Battery	21	100
	Telemetry	40	15

	Add'l wiring	26	30
Landing Gear	Nose Gear	6	26
	Main Gear	38	70
Wing	Main Spar (2)	40	44
	Leading Edge Spar (2)	30	8
	Trailing Edge Spar (2)	65	6
	Rib 1	45	9
	Rib 2	48	8
	Rib 3	51	7
	Rib 4	54	6
	Rib 5	58	5
	Rib 6	62	4
	Elevons	73	12
	Wing Covering	45	100
Fuselage	Fuselage Internal Structure	38	175
	Fuselage Covering	50	85
Payload	Tennis Ball 1	15	60
	Tennis Ball 2	15	60
	Tennis Ball 3	43	60
	Tennis Ball 4	43	60
	Golf Ball 1	27.5	46
	Golf Ball 2	27.5	46
	Ping Pong Ball 1	33.5	3
	Ping Pong Ball 2	33.5	3
	Ping Pong Ball 3	47	3
	Ping Pong Ball 4	47	3
	Ping Pong Ball 5	56	3
	Ping Pong Ball 6	56	3

Table C.3.2: COG Estimate

Mass Projection	1315	grams
Center of Gravity, MTOW	32.08	centimeters aft from propeller
Center of Gravity, Chord %	39.2%	CoG position as % of fuselage chord

Center of Gravity, Empty Weight	33.03	centimeters aft from propeller

Based on the mass properties, CAD software was used to calculate the inertia parameters:

Table C.3.3: Mass Properties

I_{xx} (kg m^2)	0.030
I_{yy} (kg m^2)	0.031
I_{zz} (kg m^2)	0.062
I_{xz} (kg m^2)	0.000

C4. Build Plan

The HALAL BWB will be built out of balsa with a MonoKote film to provide lightweight wrapping and a distinct look, as shown in Figure C.5. For the fuselage, the internal support structures (central airfoil, firewall, main and secondary spars, flooring) will all be made of balsa of varying thicknesses, as will be shown in Table C.4. The nose of the fuselage, and part of the underbelly will also be covered in thin, flexible balsa to ensure a streamlined body is heading into the wind, and the MonoKote has a smooth base to stick to.

Table C.4: Balsa Thicknesses and Uses

Thickness (in)	Use
1/16	Shell
1/8	Default: Airfoils, Winglet, Leading Edge
3/16	Central Fuselage Airfoil, Main Spar

Foam will also be used in specific locations where flexibility is needed and/or structural support is not needed from the balsa. The fuselage tail will be a block of foam glued onto the fuselage front. The elevons will be cut from foam, and the trailing edges of the wings will be sliced from foam as well.

All balsa components apart from the front shell will be laser cut, and holes will be predetermined to allow for mounting components and directing wires around (Figure C.5). This is key for the wing root airfoil (so payloads can be placed in the wing), and for the wing ribs (so that wires from the servo can be directed to the Pixhawk). The foam will be sliced using a hot-wire foam cutter.

All balsa components will also be attached using CA glue (Figure C.5). There are a few critical joints to be aware of. The main spar and ribs will be designed with deep vertical slots that allow for rigid assembly and attachment, as shown in Figure C.6. The interface between the wing and fuselage, especially towards the front, is expected to carry the most amount of stress in the structure, making the main spar assembly a key manufacturing decision. Since the wing is swept back, however, the main spar is at an angle, which reduces the number of joint options. The exact joint will be determined during build, and will be built by

hand. This introduces some risk into the design, but this risk is accepted due to time and modeling constraints. The last critical joint is the attachment of the control surface to the wing. Paper joints, glued into slots in the wing and foam elevon, will be used to keep the control surface attached. The linear actuator controlling the elevon will also provide a form of attachment, but this design has not yet been finalized.

The avionics and payload will be held in place with the following guidelines:

- Components should be attached to a central support structure where possible
- Some components (payload, battery, Pixhawk) should be placed in an accessible location, where they only move if manually moved.

As such, most avionics components will be attached to the firewall, main/secondary spar, or the Sector 2 base with screws, zip ties, or tape. Payloads will be held in place differently depending on which sector the payload is in. For Sector 1, a thin balsa strip can act as a “seatbelt” to the 2 tennis balls, placing them flush against the main spar. Sector 2 has more room available, so the exact method of holding payloads down will be determined by how the wiring is directed. However, elastic, tape, and zip ties can be used for secure attachments. Lastly, Sector 3 is just composed of payloads and is a fully enclosed sector, meaning it can serve as a basket or box without additional securing needed.

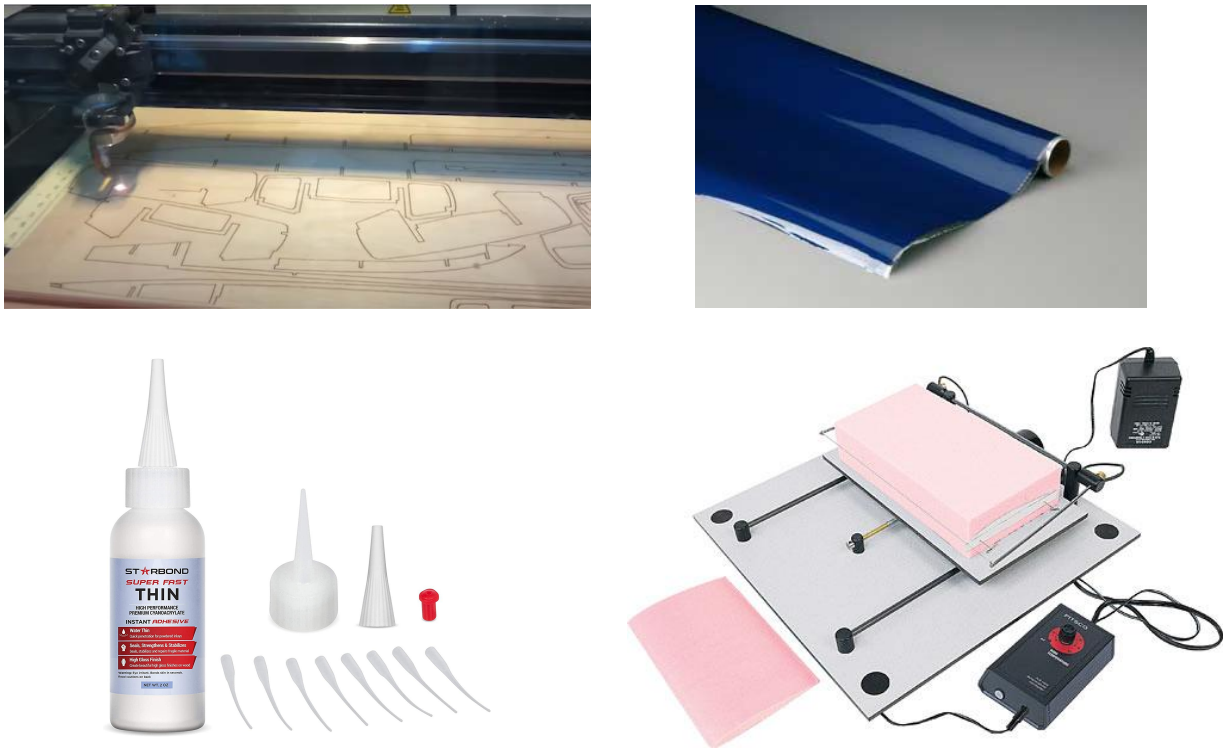

Figure C.5 *Main Build Components (External)*

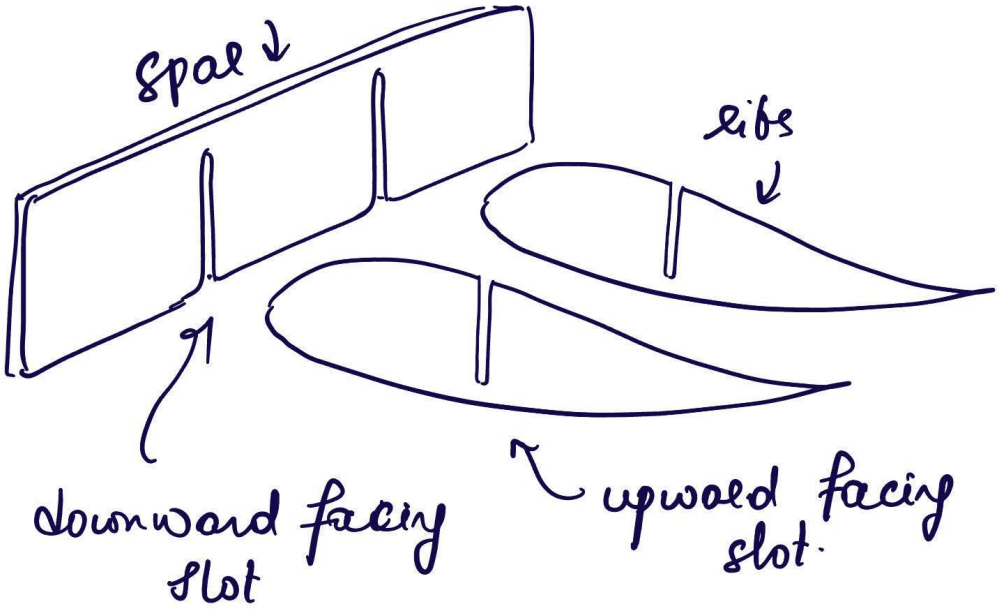

Figure C.6 *Wing Spar and Rib Joint*

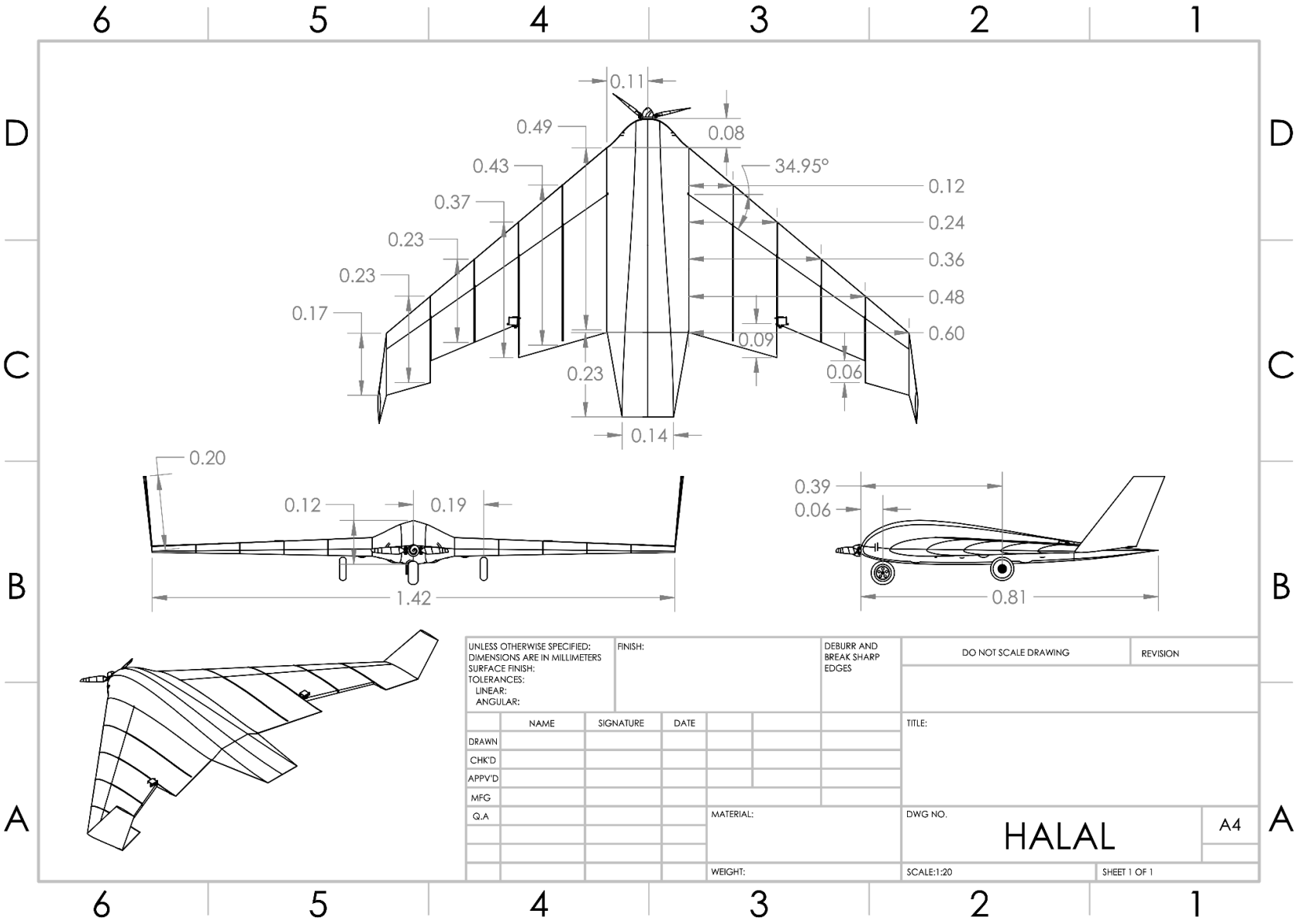

Figure C.2 *HALAL 2023 Engineering Drawing*

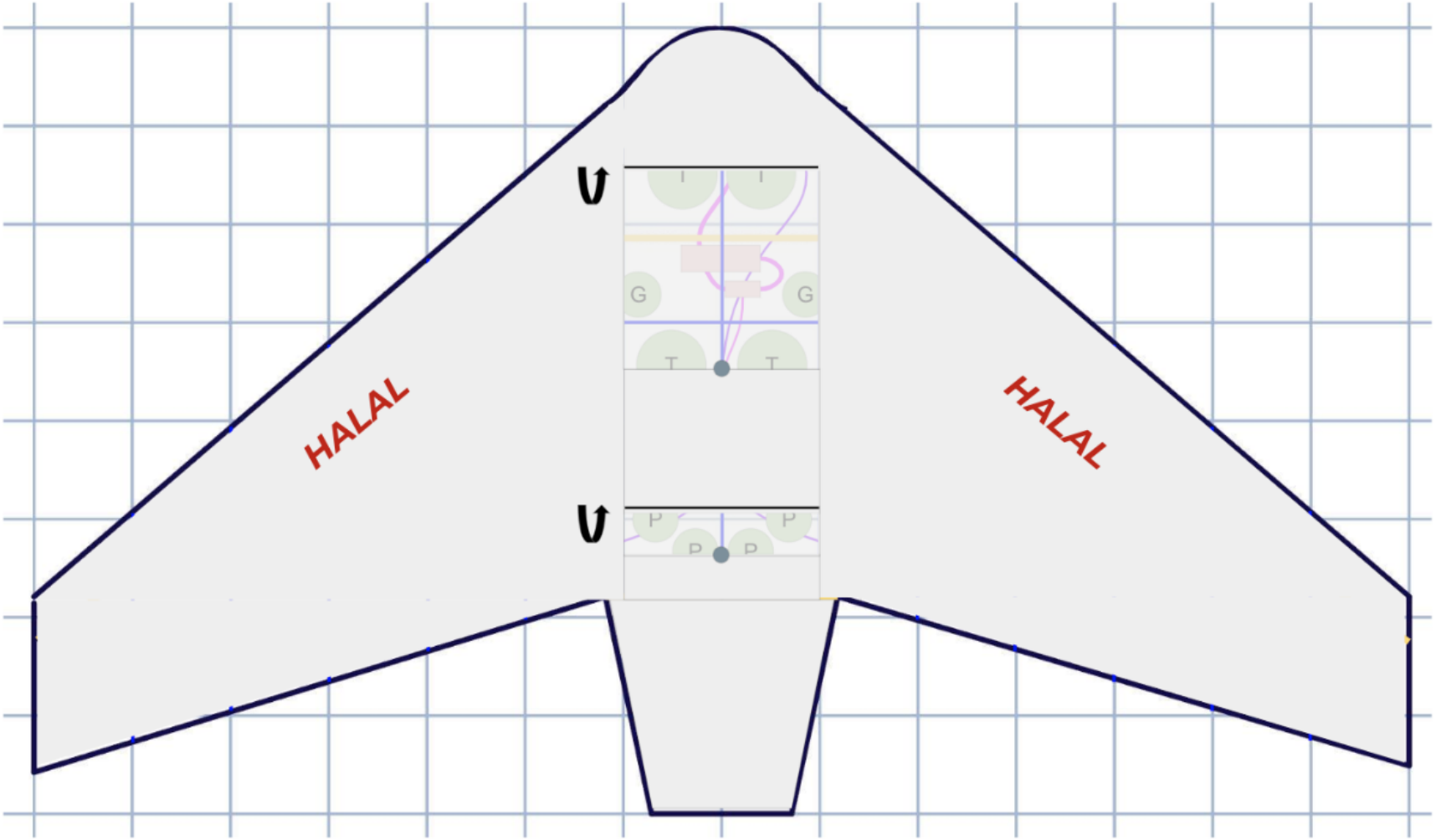

Figure C.4 *HALAL 2023 Hatch Plan*

D. Performance

D1. Performance Drivers

Some key performance drivers are listed in Table P.1.

Table P.1: Key drivers of performance criteria

Driving Factor	Performance Affected[1]	Rationale
Parasite Drag	Takeoff Performance Cruise Performance	Parasite drag is a largely invariant factor that affects all phases of flight, but reduces our efficiency in a manner that is particularly important during takeoff and cruise. Designing for a parasite drag that was as low as possible was an aerodynamic priority.
Propeller Selection	Takeoff Performance Climb Performance	Propeller selection determines how much excess thrust, and by extension power, is available at key phases of flight. Our motor, with a constant input power, produces different thrust depending on the propeller's pitch and diameter. We optimize this design choice in section D3.1.
Ground Effect	Takeoff Performance	The ground effect significantly affects our takeoff performance given the comparatively large lifting surface in close proximity to the ground. The ground effect lowers induced drag through interrupting downwash aft of the wing.
Propeller Slipstream	Takeoff Performance	The propeller slipstream represents the air flowing at a much faster rate over the central lifting surface (fuselage) in a quasi-cylinder behind the propeller. Even while stationary, air is flowing over this surface, and it creates both lifting effects and induces drag. The effects are more minor when the propeller slipstream velocity approaches the indicated airspeed of the aircraft.
Load Factor	Turning Performance High-Speed Performance	The load factor increases during accelerated operations, and increases the stall speed, as well as the thrust needed to maintain a steady turn or pull up/pull down maneuver.
Center of Moment	Cruise Performance	This, along with the center of gravity, affects the angle of attack at which level cruise can happen, and if the elevons need to be trimmed in a major way. With a large amount of trim required, the aircraft flies less 'clean,' and uses more energy to accomplish a level cruise.

[1] All performance factors are global, but these are some key phases of flight that are particularly affected.

D2. Drag Polar

The refined drag polar is seen below. This is for flight conditions, but does not consider in detail the effects of the slipstream or the propeller wash, as these effects are minimal compared to the flight speed.

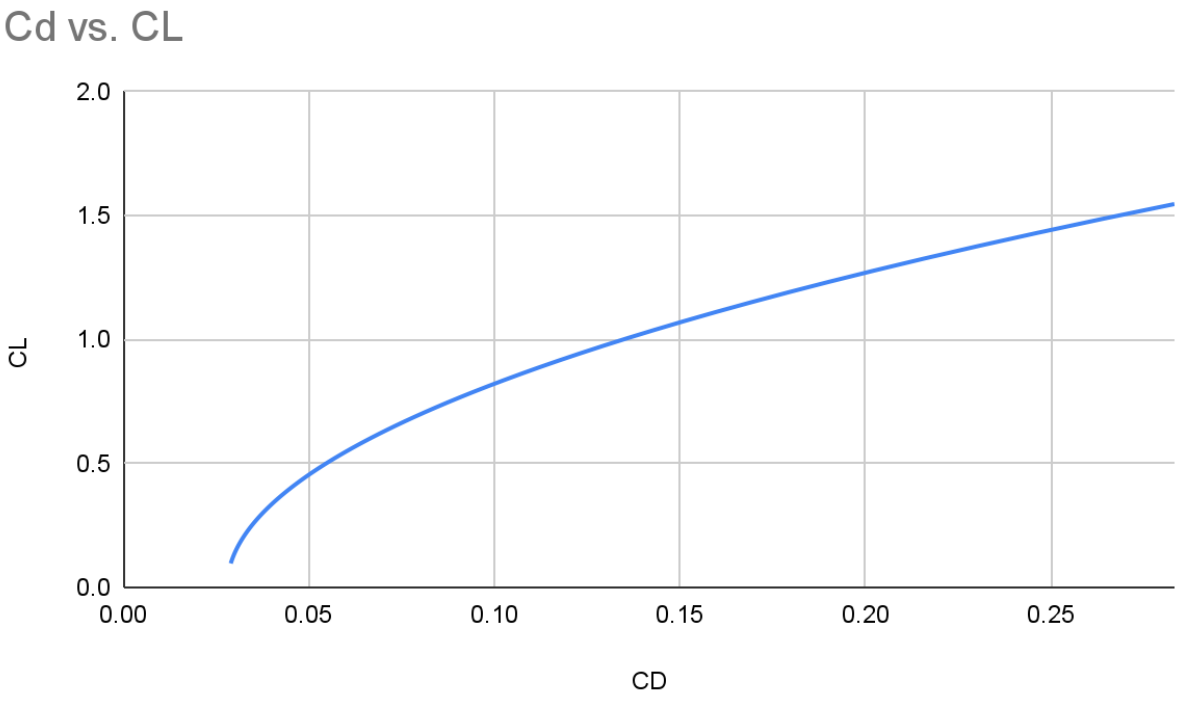

Figure P.1: Drag polar

D3. Thrust Performance

We begin our performance analysis by investigating the thrust requirement vs the thrust that can be produced by the various available propellers. The thrust required for steady, level flight is found by equating it to the aircraft's drag, assuming that L = W and T = D.

$$T_R = D = 0.5\rho V^2 S C_D \text{ where } C_D = C_{D_0} + \frac{C_L^2}{\pi AR\epsilon} \text{ [P1]}$$

The PropulsionMaxT.m code was used to generate the maximum possible thrust at a variety of airspeed conditions with three candidate propellers. The generated thrust was compared to the required thrust, and coloured as to whether significant excess thrust could be generated, less than 1 N of excess thrust could be generated, or the thrust generated was insufficient for steady, level flight. Given that the steady, level flight condition is not the condition that requires the most thrust, it is important not to choose a cruise speed where only a small amount of excess thrust is available. The below table was generated assuming 250 mAh of discharge from the battery.

Table P.2: Thrust required/generated for steady, level flight

Steady, level flight				
Cruise Speed (m/s)	**Thrust req'd [N]**	**8x8**	**9x6**	**10x5**
		Thrust generated [N]		
8.0	0.62	4.98	6.51	7.52
8.5	0.70	4.99	6.40	7.36
9.0	0.77	4.98	6.24	7.19
9.5	0.86	4.94	6.16	7.00
10.0	0.95	4.91	6.08	6.82
10.5	1.04	4.90	5.95	6.61
11.0	1.14	4.89	5.83	6.40
11.5	1.25	4.87	5.70	6.17
12.0	1.36	4.86	5.57	5.90
12.5	1.47	4.84	5.46	5.62
13.0	1.59	4.82	5.24	5.51
13.5	1.72	4.78	5.11	5.26
14.0	1.85	4.72	4.92	5.08
14.5	1.98	4.69	4.74	4.82
15.0	2.12	4.62	4.52	4.66
15.5	2.26	4.55	4.35	4.45
16.0	2.41	4.52	4.18	4.28
16.5	2.56	4.45	4.02	4.11
17.0	2.72	4.37	3.85	3.95
17.5	2.88	4.30	3.69	3.78
18.0	3.05	4.24	3.55	3.61
18.5	3.22	4.17	3.41	3.45
19.0	3.40	4.10	3.27	3.29

Not Enough Thrust	Little Excess Thrust (<1 N)	Sufficient Thrust (>1 N)

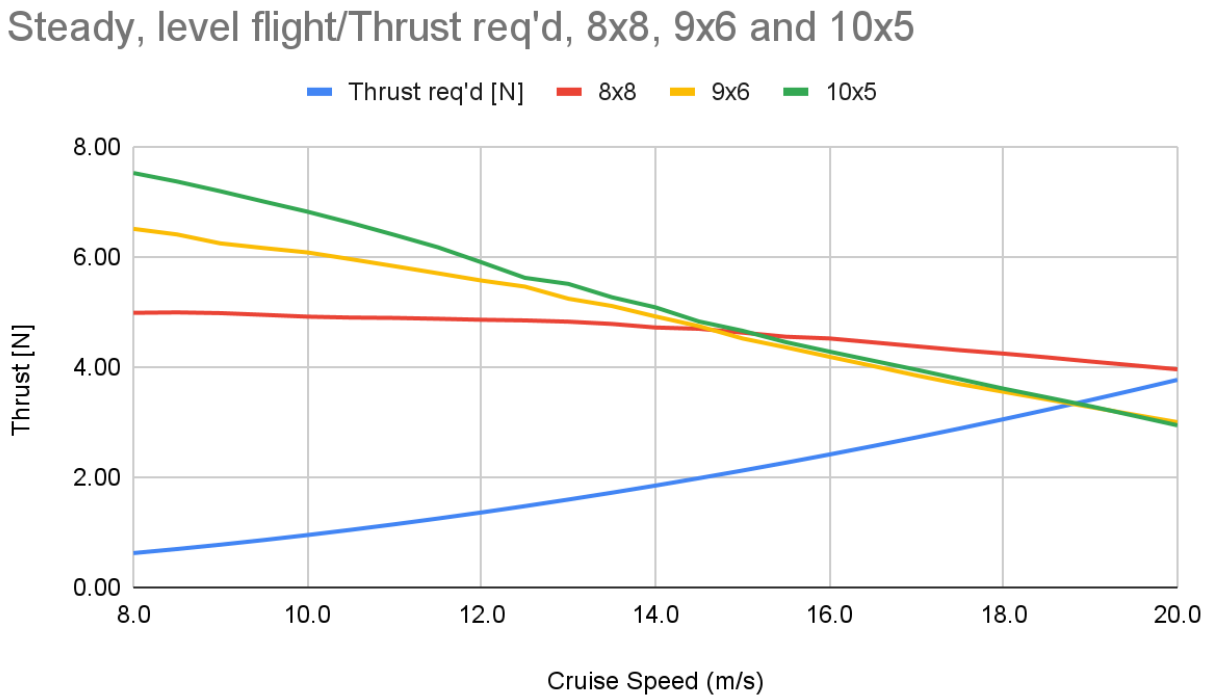

Figure P.2: Steady, level flight thrust available vs. thrust required curves

It's clear to see that aiming for a cruise speed as close to 10m/s as possible gives us the most excess thrust regardless of propeller selection. Additionally, the thrust required to maintain steady, level flight increases quickly as cruise speed increases, so it is energetically advantageous to keep the cruise speed as low as possible in addition to the direct benefits in the cost function from keeping the speed close to 10 m/s. However, the inherent variation of flight performance means that it's not entirely accurate to assume that we can cruise perfectly at 10 m/s, so we take the design cruise speed to be somewhere between 10 and 10.5 m/s. This gives sufficient room for some realistic variation in both directions without encountering a stall in a turn yet without overly reducing our excess thrust or increasing energy consumption.

1. Propeller Selection

Table P.3: Propeller tradeoff

	Thrust in cruise	**Thrust during slower maneuvers**	**Size**	**Mass**
8x8	4.9N	5N	8in diameter	19g
9x6	6.1N	6.2N	9in diameter	22g
10x5	6.8N	7.2N	10in diameter	30g

We construct a propeller tradeoff table that compares our three options. We first prioritize thrust available at cruise, and then thrust available during slower maneuvers. Thirdly, size is prioritized (lower is better),

and mass finally (lower is better). Regarding available thrust, higher is preferred but only to a point. More than several newtons of excess thrust is not necessary.

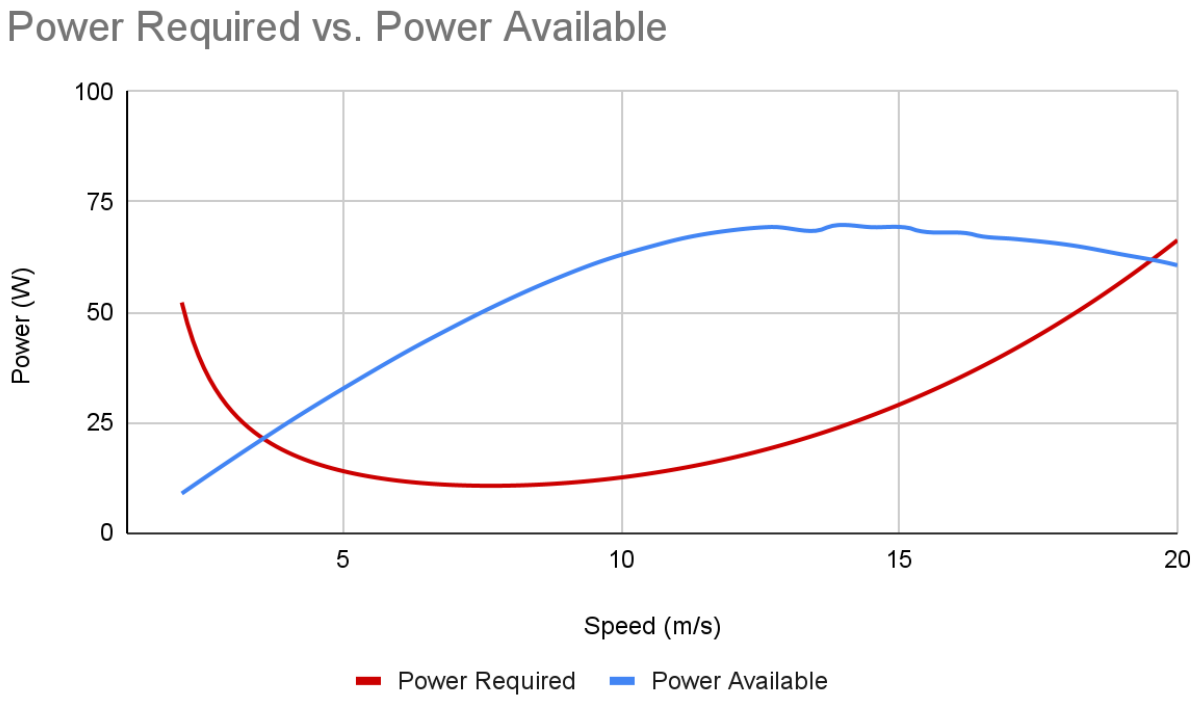

Figure P.3: Power required vs. power available

To calculate power available, we simply multiply thrust by speed, and calculate the power required by the same methodology. We climb where there is the maximum excess power. This graph additionally informs several key v-speeds below.

D4. V-Speeds

A variety of V-Speeds, or critical speeds, were calculated. Many of these are referenced directly in section D5, although some are calculated in this section where they are not clearly attributed to one flight phase.

Table P.4: Critical speeds

V-Speed	Name	Speed (m/s)
V_R	Rotation Speed	**8.46 m/s**
V_{TO}	Takeoff/Liftoff Speed	**9.31 m/s**
V_Y	Best Rate of Climb Speed	**12.4 m/s**
V_X	Best Angle of Climb Speed	**8.50 m/s**
V_{SC}	Climb Stall Speed (Pull-Up/Pull-Down)	**8.20 m/s**

V_C	Cruise Speed	**10.0 m/s**
V_E	Efficiency Speed (Minimum Power Required)	**7.95 m/s**
V_S	Stall Speed	**7.65 m/s**
V_{ST}	Turn Stall Speed (Accelerated Bank)	**8.40 m/s**
V_A	Maximum Maneuvering Speed	**16.0 m/s**
V_{APP}	Approach Speed	**10.0 m/s**
V_{TD}	Landing Speed	**8.80 m/s**
V_{ZRC}	Zero Rate of Climb Speed	**18.7 m/s**
V_{NE}	Never-Exceed Speed	**22.0 m/s**

The level flight stall speed is calculated when n = 1 in the below equation, and C_{Lmax} = 0.66. This produces a stall speed of 7.65 m/s.

$$V_s = \sqrt{\frac{2nW}{\rho S C_{L_{max}}}}$$

Maximum maneuvering speed is estimated from the structural constraints, and represents the maximum speed at which full control deflection will, within the factor of safety, be tolerated by the structure. It also represents the maximum turbulence penetration speed.

Entering a dive maneuver at V_{ZRC}:

$R_{hmin} = 7$ m

$n_{max} = 3.6$

$V_{stall} = 15$ ms^{-1}

The zero rate of climb speed is the upper intersection on the power required vs power available graphs. At this point, the aircraft will not climb at full throttle.

The never exceed speed is estimated to be the maximum speed which the structure can withstand within the appropriate factor of safety, under any flight condition, regardless of power loading. Understandably, this speed should never be passed.

D5. Flight Phase Performance Profiles

1. Takeoff

Table P.5: Takeoff Summary

	Takeoff Speed	Ground Run	Energy Consumed
Design Value:	**9.3 m/s** *Indicated airspeed*	**8.49 m** *Level dry turf runway, no headwind*	**206 J** *Level dry turf runway, no headwind*

$$V_g = \sqrt{\frac{2W}{\rho S C_{L_G}}}$$

V_g, used as rotation speed, is calculated to be 8.46 m/s, using $C_{LG} = 0.54$ as from aerodynamics calculations. $V_{LO} = 1.1V_G =$ **9.3 m/s**. We use an integral method to calculate the ground run required for takeoff. Further information is in Appendix P.1. The relevant equations are below, and ground effect (ϕ factor) is considered in the induced drag while in ground effect. Thrust is generated by the matlab codes that produced the producible thrust for various speeds.

$$\int_0^s ds = \int_{V_{hw}}^{V_{lo}} \frac{m(V - V_{hw})}{T - D - F_{fr}} dV$$

$$F_{fr} = \mu(mg - \frac{1}{2}\rho S V^2 C_L)$$

$$D_{slip} = D_{prop}\sqrt{\frac{1 + w/V}{1 + 2w/V}}$$

$$C_{wet} = \sum_i k_i c_{f_i} \frac{S_{wet_{i_{slip}}}}{S_{ref}}$$

$$D = qS_{ref}\left(C_{D_0} + \frac{\Delta q}{q}C_{wet} + KC_L^2\right)$$

$$\frac{16(h/b)^2}{1+16(h/b)^2}$$

We get a variety of takeoff distances that depend on the headwind. Of course, the takeoff speed over ground varies but the airspeed is invariant. We simply truncate the numerical integration at a higher start velocity with headwind given that air is already flowing over the stationary lifting surfaces.

Table P.6: Takeoff Data

Headwind	Ground Run	Takeoff Speed (over ground)
0.5 m/s	7.65 m	8.8 m/s
1 m/s	6.85 m	8.3 m/s
1.5 m/s	6.09 m	7.8 m/s
2 m/s	5.37 m	7.3 m/s
2.5 m/s	4.69 m	6.8 m/s
3 m/s	4.06 m	6.3 m/s

We assume that a maximum thrust is being applied during takeoff, and we calculate the power requirements with a $0.7V_{LO}$ averaging scheme. This produces a power consumption of 137 W, over a takeoff roll of up to 1.5 seconds, leading to a total energy consumption of 206 J.

Table P.7: Takeoff Operations Motor Performance

	Propeller η	Motor η	ESC η	RPM
Level Cruise	0.41	0.78	0.97	8180

2. Climb

Table P.8: Climb Summary

	Climb Speed	Rate of Climb	Energy Consumed
Design Value:	**10.2 m/s**	**3.5 m/s**	**680 J**

We assume that we will climb at the location on the curve with the most excess power, Figure P.4, which aligns well with our preferred cruise speed of 10.5 m/s. We climb slightly slower, at 10.2 m/s, to take advantage of the greatest excess power. This is not the greatest angle of attack, nor is it actually the best

rate of climb[2], but it is the greatest vertical speed that can be achieved. We anticipate that the pull-up maneuver to begin the climb could lead to a load factor of n = 1.15, which is well tolerated.

$$\frac{dh}{dt} = \frac{P_{avail} - P_{req}}{mg}$$

Using the above formula, we obtain a vertical speed of 4.02 m/s, with 52.13 W of excess power and a weight of 12.98 N. We slightly reduce this to a projected climb rate of 3.5 m/s to avoid climbing on the red line. To climb to a projected cruise altitude of 17.5 m, Halal will take 5 seconds. Using the provided Matlab codes, we calculate a power requirement of 136 W, for a total consumption of 680 J.

Table P.9: Climb Operations Motor Performance

	Propeller η	Motor η	ESC η	RPM
Level Cruise	0.57	0.78	0.97	8140

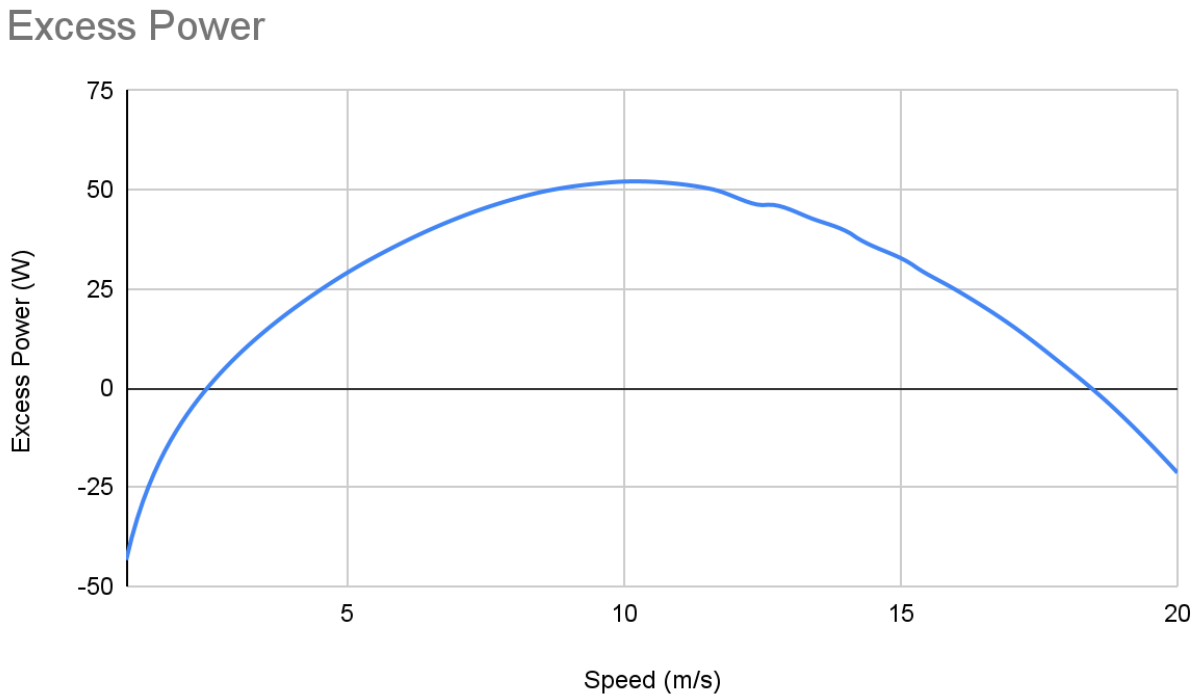

Figure P.4: Excess Power

We can also use equations from AER302 [P2] to calculate the best rate of climb speed and the best angle of climb.

[2] Considers over-ground performance as well, and is generally on the leading side of the excess power curve. A small tradeoff in vertical speed performance can lead to significant increases in over-ground performance.

$$V_{RC,\max} = \sqrt{\frac{(W/S)(T/W)}{3\rho C_{D_0}}\left(1+\sqrt{1+\frac{12KC_{D_0}}{(T/W)^2}}\right)}$$

$$\gamma_{\max} = \sin^{-1}\left(\frac{T}{W} - \frac{1}{L/D_{\max}}\right)$$

These equations lead to a best rate of climb speed of 12.45 m/s and best climb angle of 22.3 degrees respectively. The best angle of climb is achieved of 8.5 m/s.

3. Level Cruise

Table P.10: Level Cruise Summary

	Cruise Speed	Cruise Altitude	Energy Consumed
Design Value:	**10.5 m/s**	**17.5 m**	**1296 J**

We optimize our cruise speed to be as low as possible, near to 10 m/s. We design it to fly at 10.5 m/s to give us some buffer to avoid flying below 10 m/s for the cost function.

$$P_R = T_R V = qSC_{D_0} V + V\frac{W^2}{qS\pi ARe}$$

We need right about 1 N of thrust to fly at this cruise speed, in a level and steady manner. This translates to 21.6 W of power from the Matlab codes, which isn't quite the most energetically efficient speed, but is as close as we can practically get without violating the 10 m/s efficiency course constraint.

We fly 600 m in the course in a straight and level manner. At 10.5 m/s, the course will be flown in 57 seconds. This leads to an anticipated energy requirement of 1296 J.

Table P.11: Level Cruise Motor Performance

	Propeller η	Motor η	ESC η	RPM
Level Cruise	0.67	0.70	0.98	4970

4. Maneuvering/Accelerated Operations

Table P.12: Maneuvering Summary

	Maneuvering Speed	Bank Angle	Energy Consumed
Design Value:	**10.5 m/s**	**25°**	**1192 J**

Table P.13: Thrust Required for Accelerated Operations

Thrust Required	Bank Angle [degrees from level]

for Turn [N]		5	10	15	20	25	30	35	40	45
Velocity [m/s]	8.0	1.42	1.44	1.48	1.52					
	8.5	1.41	1.42	1.45	1.50	1.56	1.64			
	9.0	1.41	1.43	1.45	1.49	1.55	1.62	1.71		
	9.5	1.43	1.44	1.47	1.50	1.55	1.62	1.71	1.83	
	10.0	1.47	1.48	1.50	1.53	1.58	1.64	1.72	1.83	1.98
	10.5	1.51	1.53	1.54	1.57	1.61	1.67	1.74	1.84	1.98
	11.0	1.57	1.58	1.60	1.63	1.66	1.71	1.78	1.87	2.00
	11.5	1.64	1.65	1.67	1.69	1.72	1.77	1.83	1.92	2.03
	12.0	1.72	1.73	1.74	1.77	1.80	1.84	1.89	1.97	2.08
	12.5	1.81	1.81	1.83	1.85	1.88	1.92	1.97	2.04	2.14
	13.0	1.90	1.91	1.92	1.94	1.97	2.00	2.05	2.12	2.21
	13.5	2.00	2.01	2.02	2.04	2.06	2.10	2.14	2.20	2.29
	14.0	2.11	2.12	2.13	2.15	2.17	2.20	2.24	2.30	2.38
	14.5	2.23	2.23	2.24	2.26	2.28	2.31	2.35	2.40	2.47
	15.0	2.35	2.36	2.37	2.38	2.40	2.43	2.46	2.51	2.58

Table P.14: Turn Radii

Turn Radius [m]		Bank Angle [degrees from level]								
		5	10	15	20	25	30	35	40	45
Velocity [m/s]	8.0	74.3	36.4	23.5	16.8	12.7	9.8	7.6	6.0	4.6
	8.5	83.9	41.1	26.5	19.0	14.3	11.0	8.6	6.7	5.2
	9.0	94.0	46.1	29.8	21.3	16.0	12.4	9.7	7.5	5.8
	9.5	104.8	51.4	33.2	23.8	17.9	13.8	10.8	8.4	6.5
	10.0	116.1	56.9	36.7	26.3	19.8	15.3	11.9	9.3	7.2
	10.5	128.0	62.8	40.5	29.0	21.8	16.9	13.1	10.3	7.9
	11.0	140.4	68.9	44.5	31.8	24.0	18.5	14.4	11.3	8.7
	11.5	153.5	75.3	48.6	34.8	26.2	20.2	15.8	12.3	9.5
	12.0	167.1	82.0	52.9	37.9	28.5	22.0	17.2	13.4	10.4
	12.5	181.4	89.0	57.4	41.1	31.0	23.9	18.6	14.5	11.3
	13.0	196.2	96.2	62.1	44.5	33.5	25.8	20.2	15.7	12.2
	13.5	211.5	103.8	67.0	48.0	36.1	27.9	21.7	17.0	13.1
	14.0	227.5	111.6	72.0	51.6	38.8	30.0	23.4	18.2	14.1

	14.5	244.0	119.7	77.3	55.3	41.7	32.1	25.1	19.6	15.2
	15.0	261.2	128.1	82.7	59.2	44.6	34.4	26.8	20.9	16.2

Table P.15: Stall Speed by Bank Angle

Bank Angle [°]	**5**	**10**	**15**	**20**	**25**	**30**	**35**	**40**	**45**	**50**	**55**	**60**
Stall Speed	7.67	7.71	7.78	7.89	8.04	8.22	8.45	8.74	9.10	9.54	10.10	10.82
n	1.004	1.02	1.04	1.06	1.10	1.15	1.22	1.31	1.41	1.56	1.74	2.00

We use 1.58 N of thrust, leading to a power requirement of 33.1 W to complete a standard rate turn with a 20 m radius at 10.5 m/s. The turns account for a total of 377 m of distance to cover[3], which takes 36 seconds at 10.5 m/s. As such, 1192 J would be required to complete the standard rate turns during the efficiency flight.

Table P.16: Accelerated Operations Motor Performance

	Propeller η	**Motor η**	**ESC η**	**RPM**
25° Bank	0.65	0.74	0.98	5440

5. Approach/Landing

Table P.17: Approach/Landing Summary

	Approach Speed	**Touchdown Speed**	**Ground Run**
Design Value:	**10.0 m/s**	**8.80 m/s**	**3.5 m**

$$V_a = 1.3V_{stall}$$

$$V_{TD} = 1.15V_{stall}$$

We neglect energy requirements during the landing phase, and assume that the approach energy requirements are well-covered by the available battery. We can approximate the approach and descent

[3] 3 times πd where d = 40 m.

requirements as 80% of level cruise to have a well-controlled descent, and expect the approach to cover 200 m back to the runway. This leads to an energy consumption of 345 J.

D6. Energy Requirements

Summing the flight phases above, the indicative power consumption for the efficiency course, with a length of 977 m) will be **2488 J**. We add approximately 890 J for takeoff and climb requirements, and a further estimated 345 J for descent, leading to a total drive motor energy consumption of **3725 J** from takeoff to touchdown. This neglects power consumption by the avionics and servos, but these energy impacts are minimal by comparison.

D7. Range and Endurance

While it is clear from the battery size (~52,000 J) that range is highly in excess and the aircraft easily has enough endurance to complete the mission, it is prudent to calculate the potential range and endurance of Halal BWB. Note that E indicates the total battery energy in Joules.

$$R_{max} = \frac{\eta E}{W} \left(\frac{C_L}{C_D} \right)_{max}$$

We select a best range speed of 8.7 m/s, using the greatest ratio of C_L vs C_D; this additionally maximizes the overall propulsive efficiency (while η_{prop} and η_{motor} individually vary, their ratio is optimized here).

Using this equation, we arrive at the following parameters:

$\eta = 0.426$ (product of η_{prop}, η_{motor}, η_{ESC})
$W = 12.98$ N
$E = 51{,}948$ J
$(C_L/C_D)_{Max} = 9.15$

R_{Max} = 15,600 m, or 15.6 km in steady, level flight, with no winds.

E. Stability

E1. XFLR5 Model

To carry out the stability analysis, a model of Halal 2023 was created in XFLR5. Figure E.1 below shows the XFLR5 model used for the stability analysis.

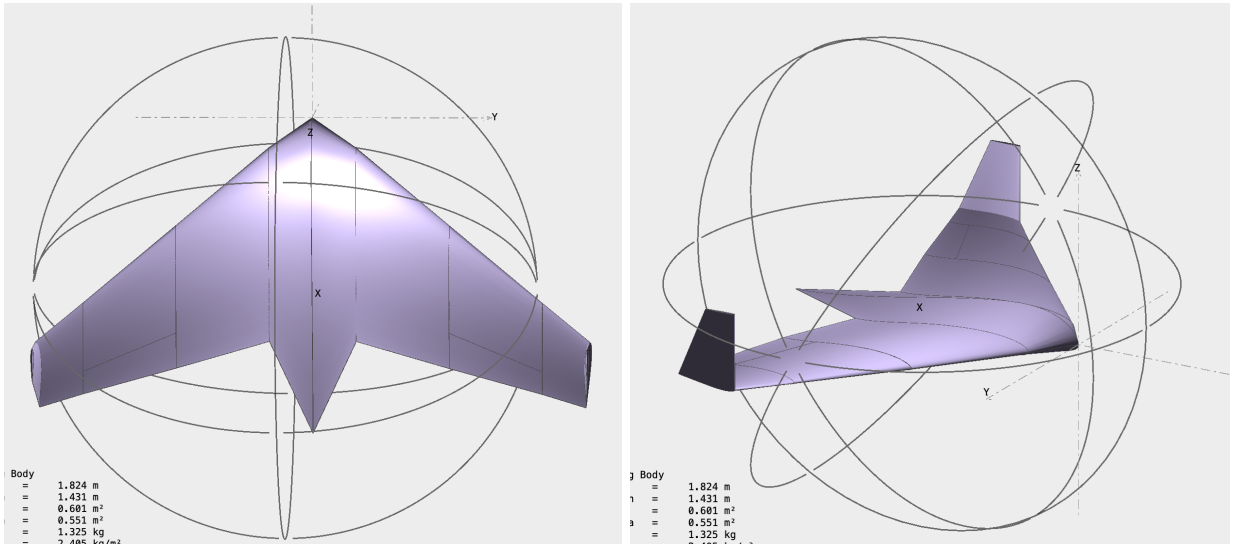

Figure E.1: XFLR5 Model of Halal 2023

E2. Static Stability

Static stability is an important concept when it comes to aircraft design. If an aircraft returns back to its desired orientation after being perturbed, it is said to have positive stability. If the aircraft remains in the perturbed state, it is said to be neutrally stable. Lastly, if the aircraft continues to move away from its equilibrium position, it is said to be statically unstable [E1].

Longitudinal Stability: This refers to an airplane's stability in the pitching plane. For positive longitudinal stability, the pitching moment coefficient with respect to the angle of attack must be negative [E2]. The longitudinal stability of various flight conditions was determined in XFLR5. Tables E.1 and E.2 summarize the graphs generated for various flight conditions, showing the pitch moment coefficient versus the angle of attack. These tables also show the lift coefficient at the trim angles for each case. Table E.1 shows the graphs for cruise conditions with full payload and no payload at a cruise speed of 10 meters per second. The red boxes in the plots show the angle of attack where the moment coefficient curve is 0. Table E.2 shows the exact same plots as Table E.1, for the take-off case, where the speed is 8.42 meters per second.

Table E.1: Cruise Conditions Longitudinal Stability

Cruise, Full Payload	Cruise, No Payload
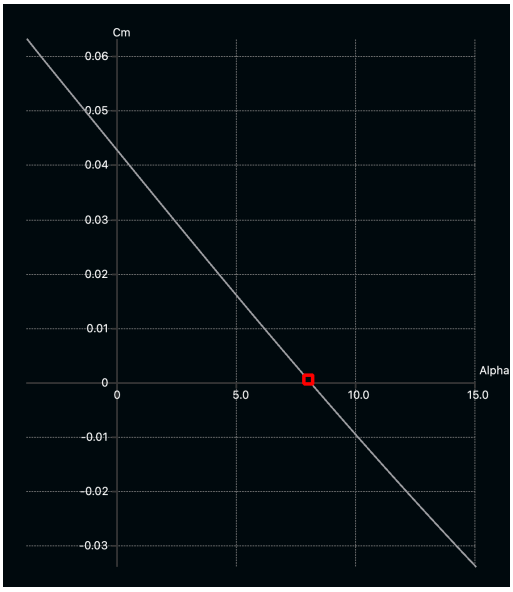	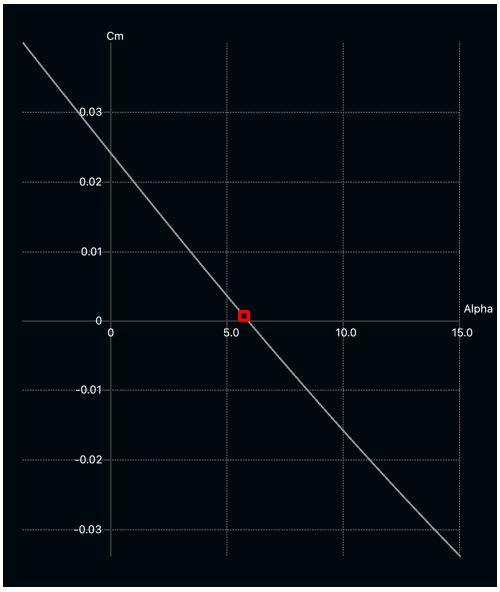
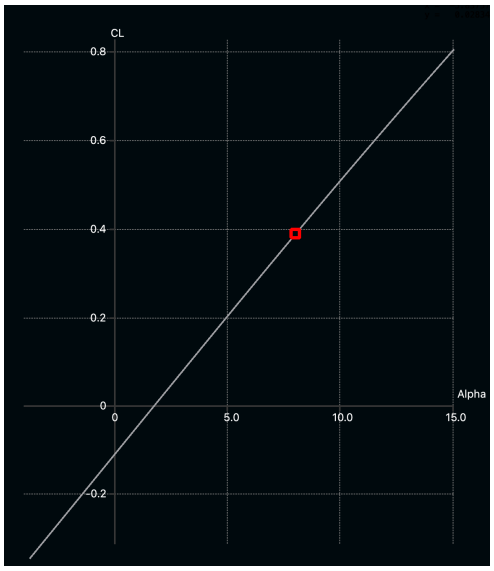	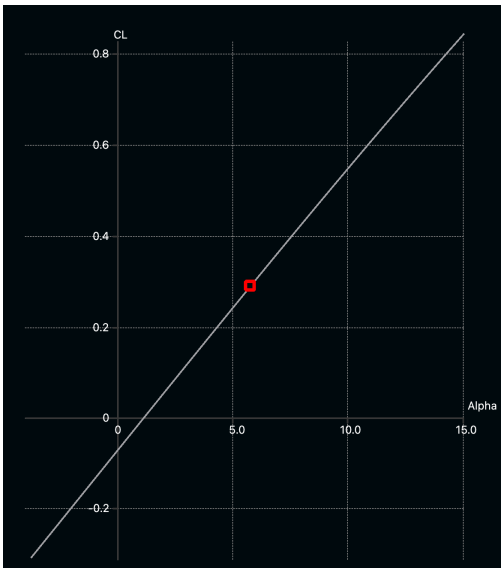

Table E.2: Takeoff Conditions Longitudinal Stability

Takeoff, Full Payload	Takeoff, No Payload
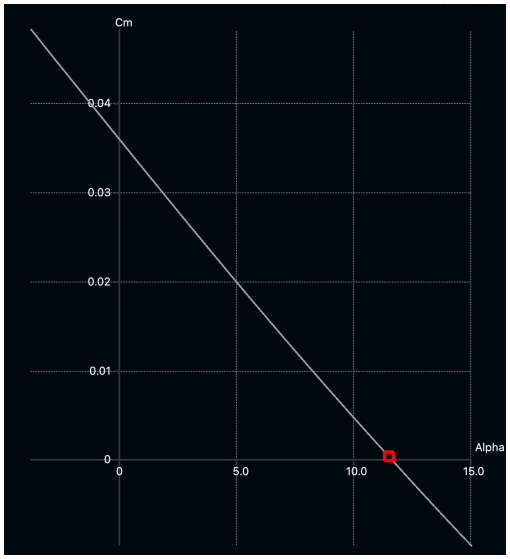	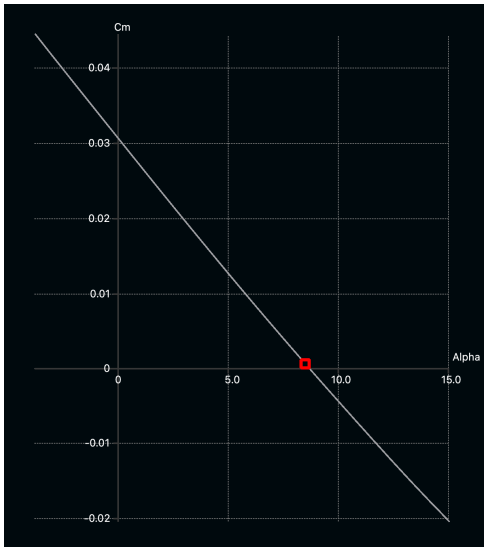
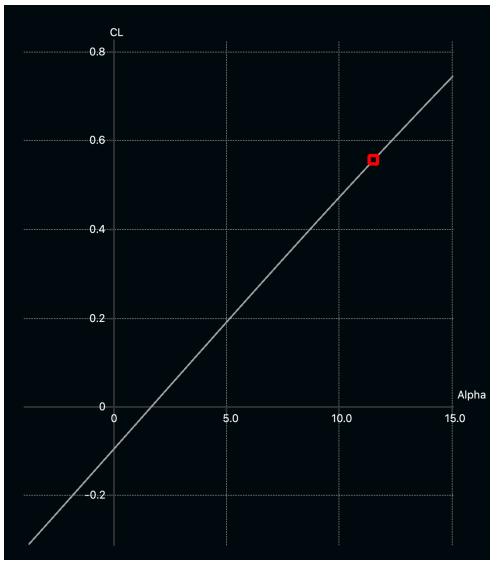	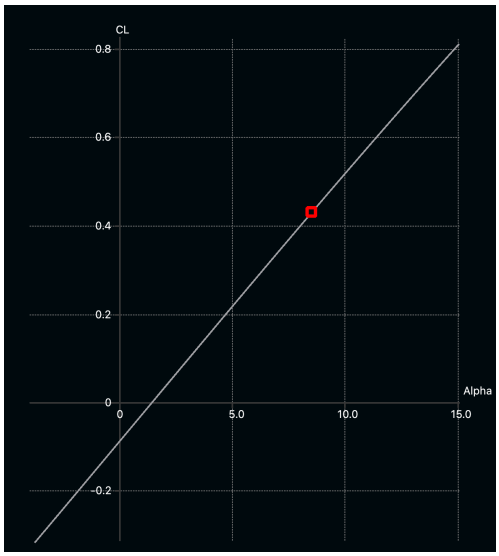

Observing Tables E.1 & E.2, it is clear that the pitching moment coefficient versus angle of attack graphs all have negative slopes, which is required for longitudinal stability. Table E.3 below summarizes the trim angles, the pitch moment coefficient derivatives obtained from the plots, lift coefficients, speeds and the elevon deflections for each case considered.

Table E.3: Pitch Moment Coefficients, Trim Angles and Elevon Deflections for Various Cases

Case	Speed	Lift Coefficient Required	Elevon Deflection	Trim Angle	C_{m_α}
Cruise, Full Payload	$10\ \frac{m}{s}$	0.39	-1.5 degrees	8 degrees	-0.00334
Cruise, No Payload	$10\ \frac{m}{s}$	0.283	1 degree	5.75 degrees	-0.00369
Takeoff, Full Payload	$8.42\ \frac{m}{s}$	0.54	-2.5 degrees	11.5 degrees	-0.00311
Takeoff, No Payload	$8.42\ \frac{m}{s}$	0.4	-1 degree	8.5 degrees	-0.00353

The pitching moment coefficients were taken about the center of gravity (CG) of the aircraft. The location of CG and the neutral point (NP) are with respect to the leading edge of the fuselage where the propeller is located. The longitudinal static margin is calculated by taking the distance between the CG and the neutral point (estimated from XFLR5) and then divided by the mean aerodynamic chord. Table E.4 summarizes the CG and NP locations, as well as the calculated static margins for each case considered.

Table E.4: Center of Gravity, Neutral Point, and Static Margin for Various Cases

Case	Center of Gravity [m]	Neutral Point [m]	Static Margin [%]
Cruise, Full Payload	0.3236	0.367	15
Cruise, No Payload	0.334	0.367	11
Takeoff, Full Payload	0.3236	0.354	10
Takeoff, No Payload	0.334	0.394	20

Lateral & Directional Stability: An aircraft that is directionally stable returns to its original position after experiencing a yawing disturbance, through the generation of a restoring yawing moment. As for a laterally stable aircraft, the rolling moment due to a disturbance in the roll direction must be negative. Lateral stability and directional stability require $C_{n\beta} > 0$ and $C_{l\beta} < 0$. Tables E.5 and S.6 show the directional and lateral stability plots, with β ranging from 0 to 10 degrees, for cruise and takeoff cases respectively. Observing these plots, it can be seen that the correct signs for the slopes are obtained.

Table E.5: Cruise Conditions Directional & Lateral Stability

Cruise, Full Payload	Cruise, No Payload
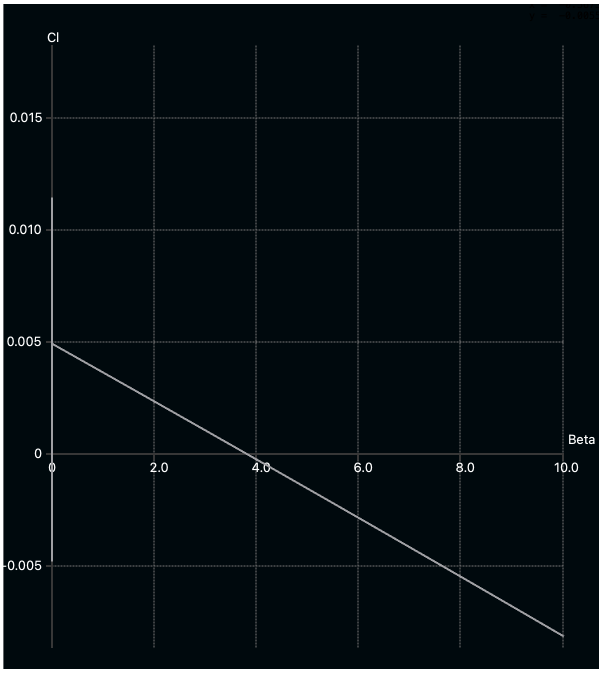	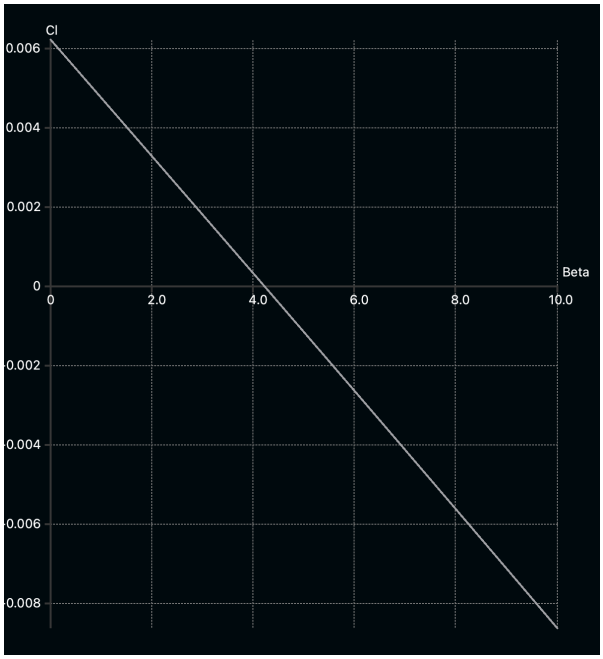
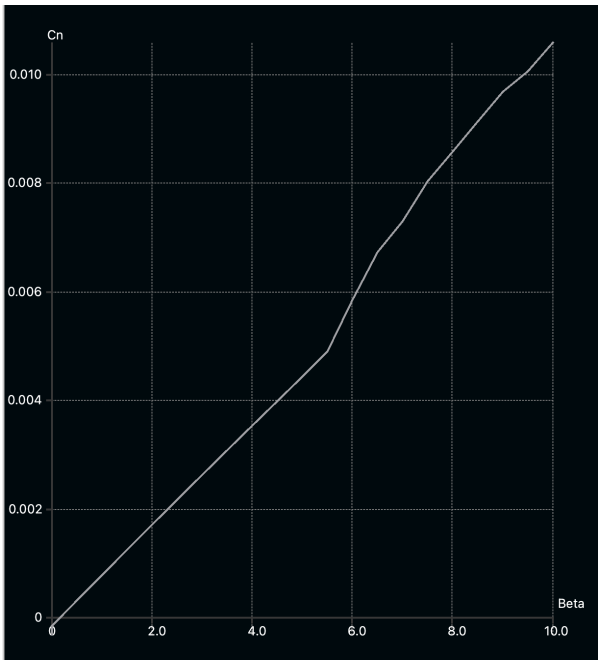	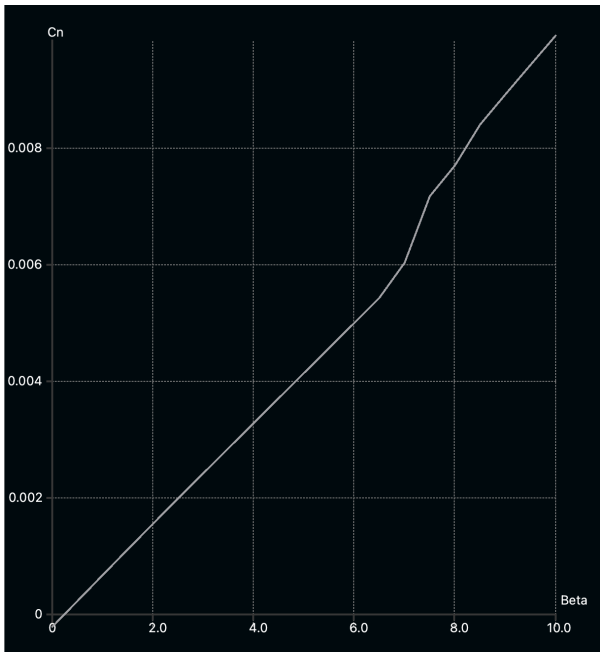

Table E.6: Takeoff Conditions Directional & Lateral Stability

Takeoff, Full Payload	Takeoff, No Payload
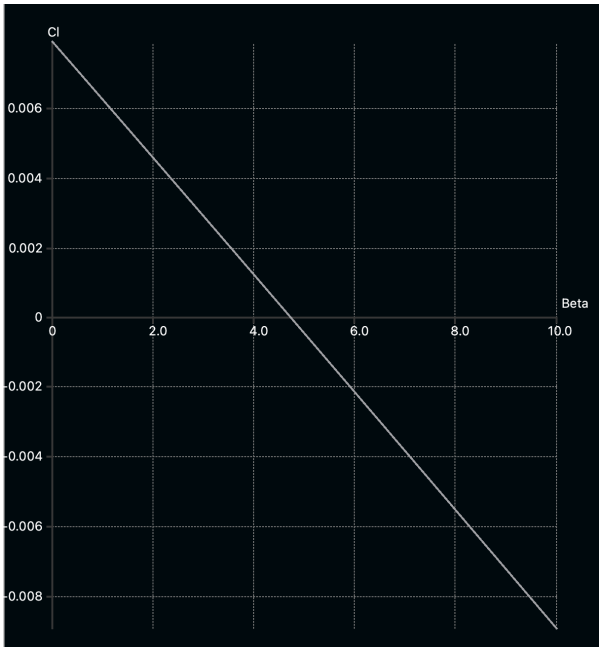	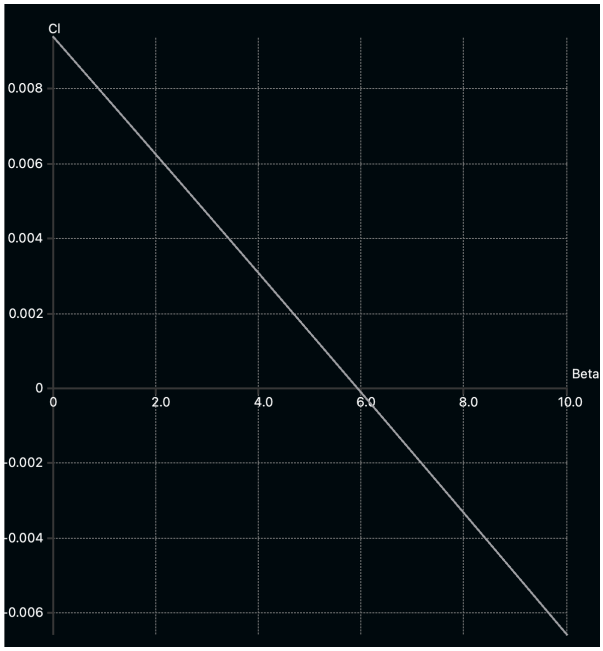
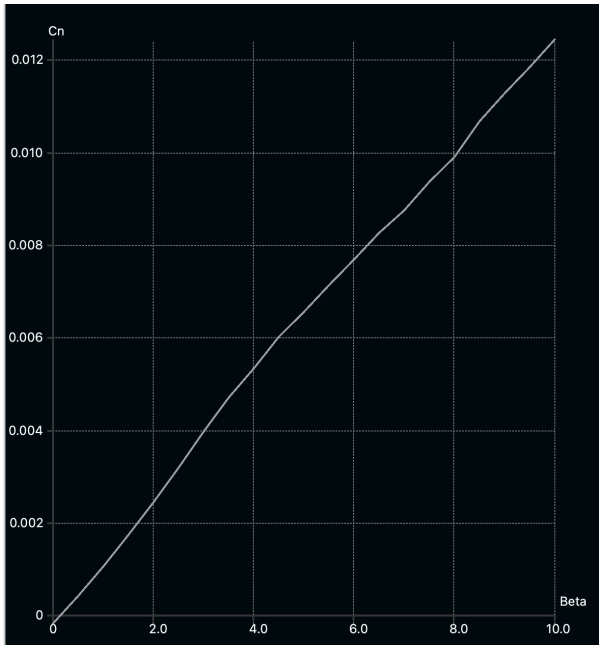	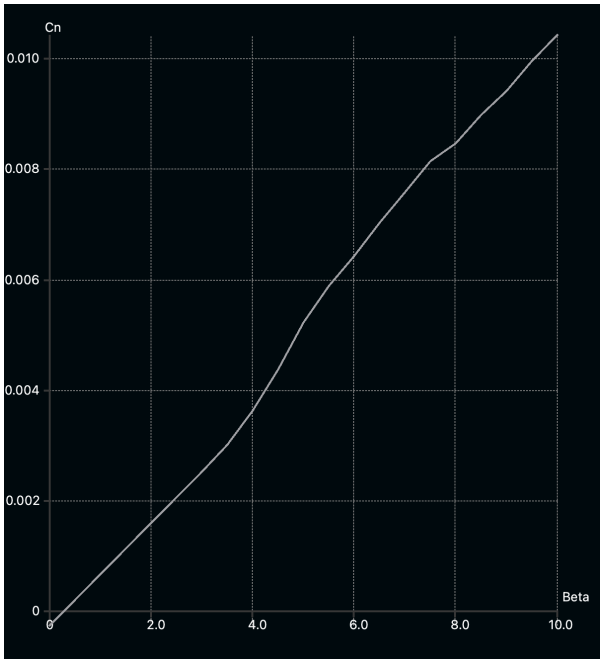

Tables E.7 below outlines the slopes of the graphs shown in Tables E.5 and E.6.

Table E.7: Directional & Lateral Stability Derivatives

Case	C_{l_β}	C_{n_β}
Cruise, Full Payload	-0.0004	0.0011
Cruise, No Payload	-0.00024	0.00097
Takeoff, Full Payload	-0.0001	0.0012
Takeoff, No Payload	-0.00028	0.0010

E3. Dynamic Stability

Dynamic stability refers to an aircraft's characteristics after a disturbance has been applied to the system, taking the time history of the motion of the aircraft into consideration [E2]. In the context of dynamic stability, different longitudinal and lateral modes are examined. The longitudinal modes considered are the short period mode and the phugoid mode, whereas the lateral modes considered are roll mode, dutch roll mode and spiral mode.

The eigenvalues, doubling time, damping and undamped frequency of the dynamic modes of the cruise conditions with full payload is shown in Table E.8. Figure E.2 shows the root locus plot for the eigenvalues of the longitudinal modes (short period and phugoid), and Figure E.3 shows the root locus plot for the eigenvalues of the lateral modes (roll, dutch roll, spiral) for the cruise, full payload case.

Table E.8: Longitudinal and Lateral Modes for Cruise, Full Payload Flight

	Eigenvalues	w_n **(frequency, rad/s)**	t_{double} **(s)**	ζ **(damping)**
Short Period	$-10 \pm 9.187i$	13.58	0.0693	0.74
Phugoid	$0.002236 \pm 1.053i$	1.053	309.9	- 0.0021
Roll	-36.93	-	0.019	-
Dutch Roll	$-1.315 \pm -7.13i$	7.25	0.526	0.18
Spiral	0.1093	-	6.3	-

From Table E.8, it can be seen that all the modes are dynamically stable except for phugoid and spiral. Short period mode is highly damped and converges fast. For the phugoid mode, since the doubling time is quite high, it can be corrected by pilot correction. Similarly for the spiral mode, since the doubling time is greater than 6 seconds, it can also be corrected by pilot correction. The short period, roll, and dutch roll modes are stable and heavily damped, and they will not lead to any issues for cruise with full payload.

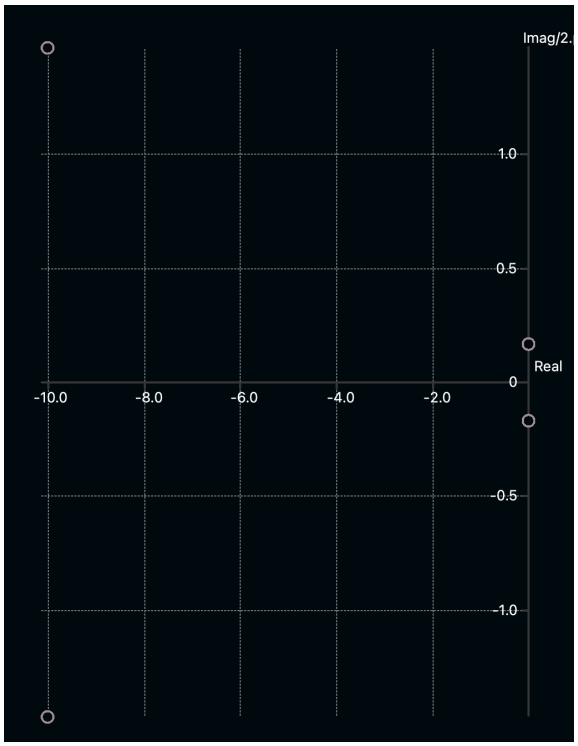

Figure E.2: Longitudinal Mode Root Locus for Cruise, Full Payload

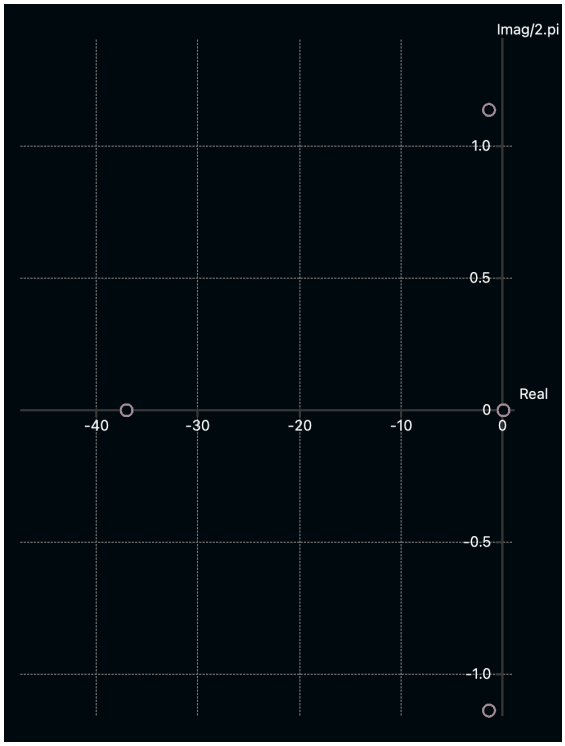

Figure E.3: Lateral Mode Root Locus for Cruise, Full Payload

The same analysis is done for the take-off case with payload, where the speed is 8.42 meters per second. Figures E.4 and E.5 show the root locus plots for the longitudinal and lateral modes for this case respectively, and Table E.9 shows the dynamic modes.

Table E.9: Longitudinal and Lateral Modes for Takeoff, Full Payload Flight

	Eigenvalues	w_n **(frequency, rad/s)**	t_{double} **(s)**	**ζ (damping)**
Short Period	$-7.717 \pm 6.354i$	9.99	0.0898	0.772
Phugoid	$-0.005353 \pm 1.193i$	1.19	129.4	0.0045
Roll	-27.94	-	0.0248	-
Dutch Roll	$-1.535 \pm -6.978i$	7.14	0.451	0.215
Spiral	0.1694	-	4.1	-

From table E.9, it can be seen that all of the modes are stable except for spiral mode. As expected, the short period is heavily damped. Unlike the cruise case, the phugoid mode is stable as well, although it is very close to the RHS in the root locus plot. The spiral mode has a doubling time of 4.1 seconds. Even though this is short, the aircraft will be at this speed for a very short amount of time during take-off, and it can most likely be handled by pilot correction.

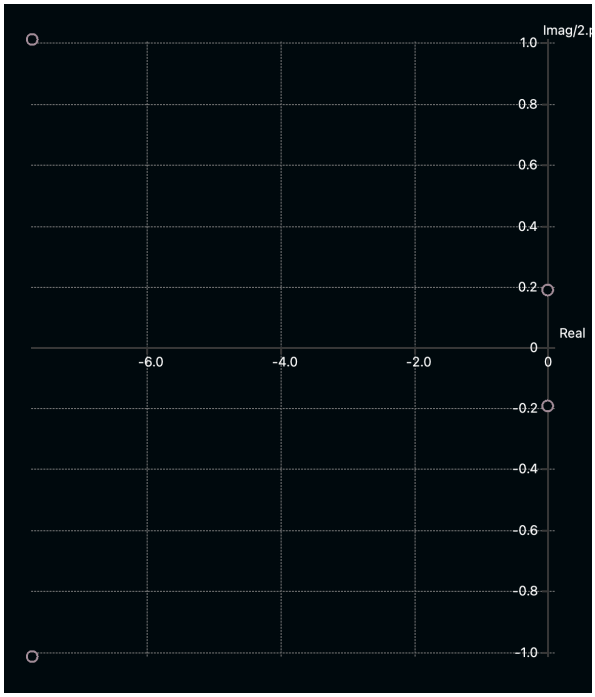

Figure E.4: Longitudinal Mode Root Locus for Takeoff, Full Payload

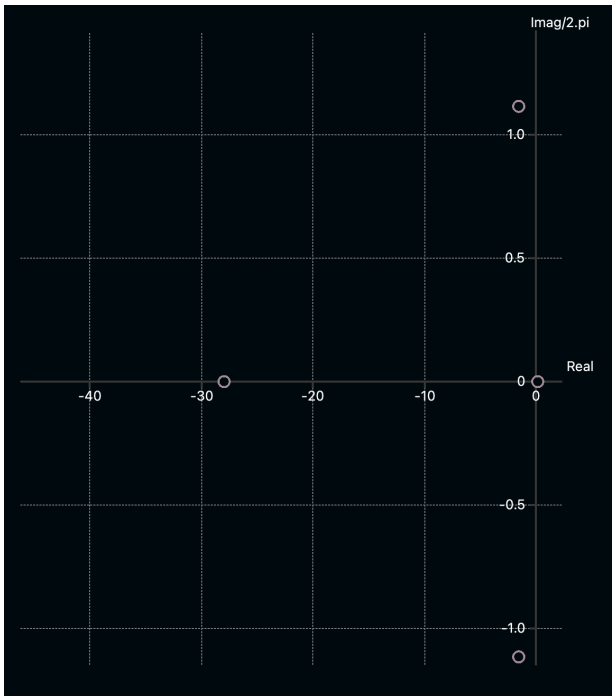

Figure E.5: Lateral Mode Root Locus for Takeoff, Full Payload

E4. Control Surface Sizing

For sizing the control surfaces, structural constraints were considered. Since the ribs are located 0.12 meters apart, the elevon's sides are designed to align with the ribs for manufacturability. Figure E.6 shows the placement of the control surfaces along the wing. The span of the control surface is 0.24 meters, such that the sides of the control surface align with ribs 3 and 5, the elevon to span ratio turns out to be 40%. As for the determination of the elevon chord to wing chord ratio, the aileron guidelines figure from Raymer was used, as shown in Figure E.7. Using this graph, for an elevon span to wing span ratio of 40%, elevon chord to wing chord ratio is between ~20 - 25 % according to historical guidelines [E3]. Various chord ratios between this range were tested, and static stability was achieved using all tests. Since a major difference was not observed between chord ratios of 20 -25%, a maximum elevon chord to wing chord ratio of 25% was chosen. This resulted in the dimensions as shown in Figure S.6 for the control surface. The area of each control surface is 0.018 meters squared, with a mean chord of 0.0755 meters and a span of 0.24m.

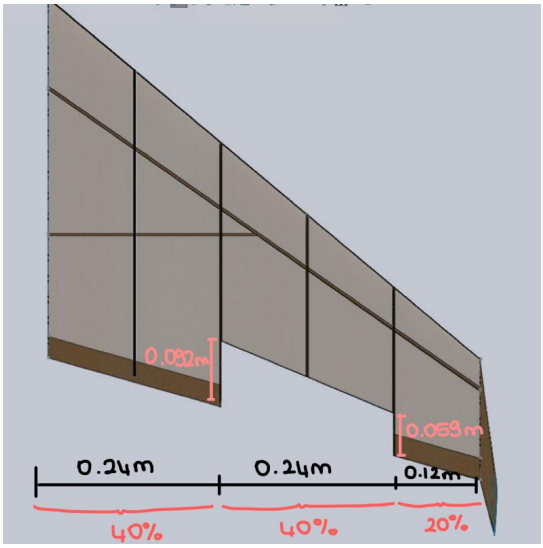

Figure E.6: Control Surface Sizing

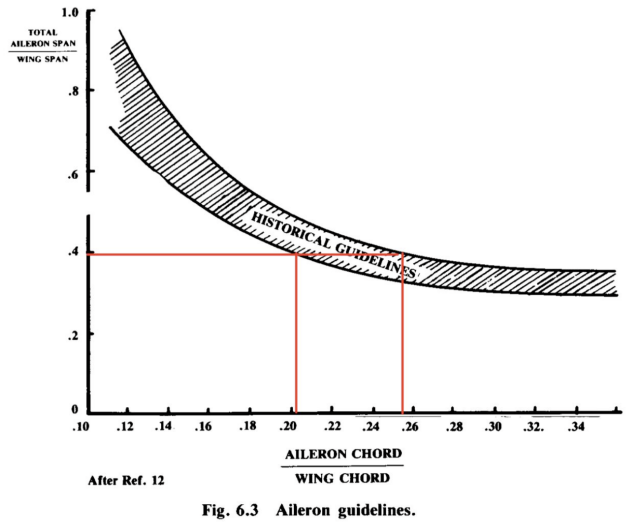

Figure E.7: Raymer's Aileron Guidelines [E3]

E5. Maximum Hinge Moment

The hinge moments can be calculated using the following formula:

$H_i = 0.5\,x\,V^2\,x\,S_i\,x\,\rho\;x\,\bar{c}_i\;x\,C_{h_i}$ where S_i is the area of the control surface, $\bar{c}_i$ is the aerodynamic chord of the control surface, V is the speed, C_{h_i} is the hinge moment coefficient and ρ is the density. Halal 2023 has two identical control surfaces, where the aerodynamic chord is 0.0755 meters and the area is 0.01812. *Table E.10* shows the hinge moment calculations for cruise with full payload, takeoff with full payload, turn with full payload (where bank is 25 degrees). The hinge moment coefficients in this table are obtained from XFLR5. The servo actuator (Hitec HS-65 HB) has a maximum torque of 0.186 N.m [E4]. As shown in *Table E.10* the maximum hinge moments are within the limits of the torque that can be provided by the servos.

Table E.10: Hinge Moment

Case	C_{h_i}	$\rho\ (\frac{kg}{m^3})$	$V\ (\frac{m}{s})$	$S_i\ (m)$	$\bar{c}_i\ (m)$	$H_i\ (N.m)$
Cruise	0.0001	1.225	10	0.01812	0.0755	$8.38\,x\,10^{-6}$
Takeoff	0.00075	1.225	8.42	0.01812	0.0755	$4.46\,x\,10^{-5}$
Turn	0.000125	1.225	10	0.01812	0.0755	$1.05\,x\,10^{-5}$

Appendices

Appendix A.1 Cargo Units Tradeoff

The driving elements for cargo load estimation at this design phase were maximizing the points obtained for the cargo units, and aiming for PF=0.25 as closely as possible, as in the first section. Using the best estimate we could from the previous successful missions, we approximated 300-350g as a reasonable mass to allocate to payload, designing slightly conservatively to permit for mass growth allowance.

We viewed ping pong balls as bonuses to fill space, but not the primary target. First, we optimized the number of golf balls and tennis balls. We could then use ping pong balls to fill any remaining mass or volume.

Payload	Max Allowed	Points Per	Diameter (mm)	Mass (g)
Ping Pong	8	10	40	2.7
Golf	8	50	42.7	45.9
Tennis	4	100	65.4 - 68.6	56 - 59.4*

Cargo Load Options (Round 1)

Option	No. Golf	No. Tennis	No. of Payload Balls	Total Mass	Cargo Units	Notes
1	0	4	4	237.6	400	
2	1	4	5	283.5	450	
3	2	3	5	270	400	
4	3	3	6	315.9	450	If max. points is the goal
5	4	2	6	302.4	400	Happy medium
6	6	0	6	275.4	300	If min. mass is the goal (aircraft performance)
7	7	0	7	321.3	350	If max. cargo units is the goal (direct to FS)

Cargo Load Options (Round 2)

ID	No. Golf	No. Tennis	No. of Payload Balls	Total Mass	Leftover mass for Ping Pong Balls	No. Ping Pong	Total No. of Balls	Total Mass	Total Cargo Units
1	0	4	4	237.6	81.15	30	34	318.6	700
2	1	4	5	283.5	35.25	13	18	318.6	580
3	2	3	5	270	48.75	18	23	318.6	580
4	3	3	6	315.9	2.85	1	7	318.6	460
5	4	2	6	302.4	16.35	6	12	318.6	460
6	6	0	6	275.4	43.35	16	22	318.6	460
7	7	0	7	321.3	-2.55	-1	6	318.6	340

Options 1-3: Too many ping pong balls, violates constraint.
Option 4: Could be considered, but is not preferred due to odd numbers of balls which could make roll stability challenging with cargo storage locations.
Option 5: Allows for maximum mass and acceptable number of cargo points
Option 6: Too many ping pong balls, violates constraint
Option 7: <0 ping pong balls, not realistic

We moved forward with a plan to use **4 tennis balls** and **2 golf balls,** as well as **6 ping pong balls**.

Appendix C.1 Spar Sizing

Assuming an elliptical lift distribution, a load factor of 3.6 (D4), and a rectangular cross-section, a max stress σ_{max} = 5.598 MPa is obtained, which is much lower than the yield strength of balsa wood (3.71 GPa). The exact calculations for bending moments can be found below. For this iteration, a spar height = wing thickness = 0.05m was selected. This is 26.9% of the chord of the airfoil that joins the wing to the fuselage. Similarly, a spar width of half the wing thickness = 3mm was used.

$$M(y) = \frac{n\,W}{6b^2\pi}\left[nb^2\sqrt{b^2-4y^2} - \left(b^2-4y^2\right)^{\frac{3}{2}} + 6b^2 y \arcsin\left(\frac{2y}{b}\right) + 3\pi b^2 y\right]$$

$$M(0) = M_{\max} = \frac{nWb}{3\pi}$$

$$= \frac{3.6}{3}\frac{1.315 \times 9.81 \times 1.42}{\pi}$$

$$= 6.997\,Nm$$

$$\sigma_{\max} = \frac{Mc_{\max}}{I} = M \times \frac{h}{2} \times \frac{12}{wh^3} = \frac{6M}{wh^2} = 5.598\,MPa$$

Where c = length of the bottom member, which is different from the rectangular cross-section.

To further validate this design decision, the maximum deflection was calculated. The spar tapers due to the change in wing thickness, as shown in the figure below. The max deflection is 0.0023m = 0.23cm. Since the deflection should be < 10% of the beam length = 0.1 * 0.736m = 0.0736m, the max deflection calculated is acceptable. The Elastic Modulus was found on the Wood Database.

$$I_y = \frac{h^3 b}{12} = \frac{0.03^3 \times 0.003}{12} = 6.75 \times 10^{-9}$$

$$\delta_{\max} = \frac{wL^4}{8EI} = \frac{1.315 \times 9.81 \times 0.73^4}{8 \times 3.71 \times 10^9 \times 6.75 \times 10^{-9}} = 0.018m = 1.82\,cm$$

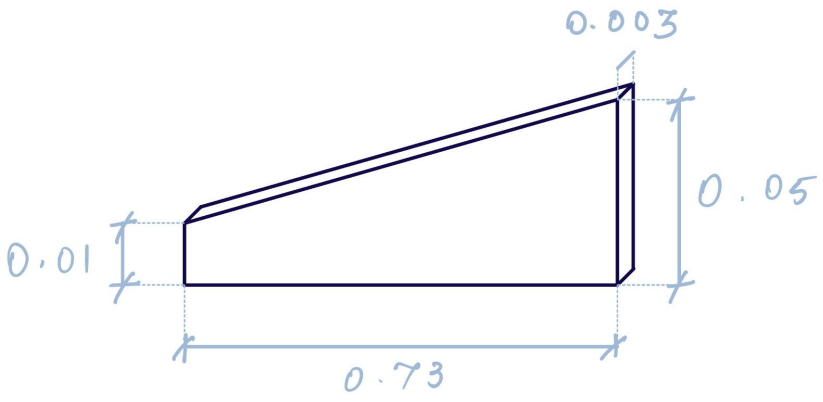

Figure: Main Spar Taper (Not to scale)

Appendix D.1 Takeoff Calculations

Takeoff Calculations Numerical Integration Results

Headwind	0.5000	m/s	Vto	9.2000	
m	1.3250	kg	Takeoff Run (m, ft)	**7.6536**	**25.1114**
W	12.9983	N			
mu_g	0.0300				
rho	1.2930				
S	0.5200				
k	0.1038				
phi	0.4553				

Takeoff Calculations Numerical Integration

Speed	**T**	**Ffr**	**CD0**	**CL**	**w**	**Dslip**	**Cwet**	**q**	**D_cl**	**Integral**
0.500	8.927	0.389	0.028	0.550	14.847	16.298	0.002	0.162	0.319	0.000
0.600	8.916	0.388	0.028	0.540	14.766	16.325	0.002	0.233	0.319	0.002
0.700	8.904	0.387	0.028	0.540	14.686	16.352	0.002	0.317	0.320	0.003
0.800	8.892	0.386	0.028	0.540	14.607	16.378	0.002	0.414	0.322	0.005
0.900	8.880	0.386	0.028	0.540	14.528	16.405	0.002	0.524	0.323	0.006
1.000	8.867	0.385	0.028	0.540	14.450	16.433	0.002	0.647	0.325	0.008
1.100	8.854	0.383	0.028	0.540	14.373	16.460	0.002	0.782	0.328	0.010
1.200	8.841	0.382	0.028	0.540	14.297	16.487	0.002	0.931	0.330	0.011
1.300	8.827	0.381	0.028	0.540	14.221	16.514	0.002	1.093	0.333	0.013
1.400	8.813	0.379	0.028	0.540	14.145	16.541	0.002	1.267	0.336	0.015
1.500	8.799	0.378	0.028	0.540	14.071	16.568	0.002	1.455	0.340	0.016
1.600	8.784	0.376	0.028	0.540	13.996	16.596	0.002	1.655	0.343	0.018
1.700	8.769	0.374	0.028	0.540	13.923	16.623	0.002	1.868	0.347	0.020
1.800	8.754	0.372	0.028	0.540	13.850	16.650	0.002	2.095	0.352	0.021
1.900	8.739	0.370	0.028	0.540	13.777	16.678	0.002	2.334	0.356	0.023
2.000	8.724	0.368	0.028	0.540	13.705	16.705	0.002	2.586	0.361	0.025
2.100	8.708	0.366	0.028	0.540	13.633	16.732	0.002	2.851	0.367	0.027
2.200	8.692	0.364	0.028	0.540	13.562	16.760	0.002	3.129	0.372	0.028
2.300	8.676	0.361	0.028	0.540	13.491	16.787	0.002	3.420	0.378	0.030
2.400	8.660	0.359	0.028	0.540	13.420	16.815	0.002	3.724	0.384	0.032
2.500	8.644	0.356	0.028	0.540	13.350	16.842	0.002	4.041	0.390	0.034
2.600	8.627	0.353	0.028	0.540	13.280	16.870	0.002	4.370	0.397	0.035

2.700	8.611	0.350	0.028	0.540	13.210	16.897	0.002	4.713	0.404	0.037
2.800	8.594	0.347	0.028	0.540	13.140	16.925	0.002	5.069	0.411	0.039
2.900	8.578	0.344	0.028	0.540	13.071	16.952	0.002	5.437	0.419	0.041
3.000	8.561	0.341	0.028	0.540	13.003	16.980	0.002	5.819	0.426	0.043
3.100	8.542	0.338	0.028	0.540	12.938	17.007	0.002	6.213	0.435	0.044
3.200	8.522	0.334	0.028	0.540	12.875	17.034	0.002	6.620	0.443	0.046
3.300	8.502	0.331	0.028	0.540	12.815	17.062	0.002	7.040	0.452	0.048
3.400	8.480	0.327	0.028	0.540	12.755	17.089	0.002	7.474	0.461	0.050
3.500	8.459	0.323	0.028	0.540	12.696	17.116	0.002	7.920	0.471	0.052
3.600	8.438	0.319	0.028	0.540	12.637	17.143	0.002	8.379	0.481	0.054
3.700	8.417	0.315	0.028	0.540	12.577	17.170	0.002	8.851	0.491	0.056
3.800	8.396	0.311	0.028	0.540	12.518	17.197	0.002	9.335	0.501	0.058
3.900	8.375	0.307	0.028	0.540	12.459	17.224	0.002	9.833	0.512	0.060
4.000	8.353	0.303	0.028	0.540	12.401	17.250	0.002	10.344	0.523	0.062
4.100	8.332	0.298	0.028	0.540	12.343	17.277	0.002	10.868	0.534	0.064
4.200	8.311	0.294	0.028	0.540	12.285	17.304	0.002	11.404	0.545	0.066
4.300	8.290	0.289	0.028	0.540	12.226	17.331	0.002	11.954	0.557	0.068
4.400	8.270	0.285	0.028	0.540	12.167	17.358	0.002	12.516	0.569	0.070
4.500	8.250	0.280	0.028	0.540	12.106	17.385	0.002	13.092	0.581	0.072
4.600	8.230	0.275	0.028	0.540	12.046	17.412	0.002	13.680	0.594	0.074
4.700	8.211	0.270	0.028	0.540	11.985	17.439	0.002	14.281	0.606	0.076
4.800	8.191	0.264	0.028	0.540	11.926	17.466	0.002	14.895	0.619	0.078
4.900	8.170	0.259	0.028	0.540	11.868	17.493	0.002	15.522	0.633	0.080
5.000	8.149	0.254	0.028	0.540	11.812	17.519	0.002	16.163	0.646	0.082
5.100	8.127	0.248	0.028	0.540	11.758	17.546	0.002	16.815	0.661	0.084
5.200	8.103	0.243	0.028	0.540	11.707	17.572	0.002	17.481	0.675	0.087
5.300	8.079	0.237	0.028	0.540	11.658	17.598	0.002	18.160	0.690	0.089
5.400	8.054	0.231	0.028	0.540	11.609	17.624	0.002	18.852	0.705	0.091
5.500	8.030	0.225	0.028	0.540	11.562	17.649	0.002	19.557	0.720	0.094
5.600	8.005	0.219	0.028	0.540	11.515	17.675	0.002	20.274	0.736	0.096
5.700	7.980	0.213	0.028	0.540	11.468	17.700	0.002	21.005	0.752	0.098
5.800	7.956	0.207	0.028	0.540	11.420	17.726	0.002	21.748	0.768	0.101
5.900	7.932	0.200	0.028	0.540	11.372	17.751	0.002	22.505	0.785	0.103
6.000	7.909	0.194	0.028	0.540	11.323	17.777	0.002	23.274	0.802	0.105
6.100	7.885	0.187	0.028	0.540	11.275	17.802	0.002	24.056	0.819	0.108

6.200	7.861	0.181	0.028	0.540	11.227	17.828	0.002	24.851	0.836	0.110
6.300	7.838	0.174	0.028	0.540	11.180	17.853	0.002	25.660	0.854	0.113
6.400	7.813	0.167	0.028	0.540	11.134	17.878	0.002	26.481	0.872	0.115
6.500	7.789	0.160	0.028	0.540	11.090	17.903	0.002	27.315	0.890	0.118
6.600	7.764	0.153	0.028	0.540	11.047	17.927	0.002	28.162	0.909	0.121
6.700	7.738	0.145	0.028	0.540	11.005	17.952	0.002	29.021	0.928	0.123
6.800	7.712	0.138	0.028	0.540	10.965	17.976	0.002	29.894	0.947	0.126
6.900	7.686	0.131	0.028	0.540	10.925	18.000	0.002	30.780	0.966	0.129
7.000	7.659	0.123	0.028	0.540	10.887	18.024	0.002	31.678	0.986	0.131
7.100	7.632	0.115	0.028	0.540	10.850	18.047	0.003	32.590	1.007	0.134
7.200	7.605	0.108	0.028	0.540	10.814	18.071	0.003	33.515	1.027	0.137
7.300	7.578	0.100	0.028	0.540	10.780	18.094	0.003	34.452	1.048	0.140
7.400	7.550	0.092	0.028	0.540	10.747	18.117	0.003	35.402	1.069	0.143
7.500	7.521	0.084	0.028	0.540	10.716	18.139	0.003	36.366	1.091	0.146
7.600	7.492	0.075	0.028	0.540	10.687	18.161	0.003	37.342	1.113	0.149
7.700	7.462	0.067	0.028	0.540	10.659	18.183	0.003	38.331	1.135	0.152
7.800	7.433	0.059	0.028	0.540	10.631	18.205	0.003	39.333	1.157	0.156
7.900	7.404	0.050	0.028	0.540	10.605	18.226	0.003	40.348	1.180	0.159
8.000	7.374	0.041	0.028	0.540	10.579	18.248	0.003	41.376	1.203	0.162
8.100	7.344	0.033	0.028	0.540	10.554	18.269	0.003	42.417	1.227	0.165
8.200	7.314	0.024	0.028	0.540	10.531	18.290	0.003	43.471	1.251	0.169
8.300	7.283	0.015	0.028	0.540	10.511	18.310	0.003	44.537	1.275	0.172
8.400	7.251	0.006	0.028	0.540	10.494	18.330	0.003	45.617	1.300	0.176
8.500	7.218	-0.004	0.028	0.540	10.479	18.349	0.003	46.710	1.325	0.180
8.600	7.184	-0.013	0.028	0.540	10.469	18.367	0.003	47.815	1.350	0.184
8.700	7.149	-0.022	0.028	0.540	10.463	18.385	0.003	48.934	1.376	0.187
8.800	7.114	-0.032	0.028	0.540	10.459	18.403	0.003	50.065	1.402	0.191
8.900	7.078	-0.041	0.028	0.540	10.457	18.420	0.003	51.209	1.429	0.196
9.000	7.041	-0.051	0.028	0.540	10.458	18.436	0.003	52.366	1.456	0.200
9.100	7.004	-0.061	0.028	0.540	10.460	18.452	0.003	53.537	1.484	0.204
9.200	6.967	-0.071	0.028	0.540	10.465	18.468	0.003	54.720	1.512	0.209
9.300	6.929	-0.081	0.028	0.540	10.472	18.483	0.003	55.916	1.540	0.213
9.400	6.892	-0.091	0.028	0.540	10.479	18.498	0.003	57.125	1.568	0.218
9.500	6.855	-0.102	0.028	0.540	10.485	18.514	0.003	58.347	1.597	0.223
9.600	6.819	-0.112	0.028	0.540	10.491	18.529	0.003	59.581	1.626	0.227

9.700	6.783	-0.122	0.028	0.540	10.498	18.543	0.003	60.829	1.656	0.232
9.800	6.747	-0.133	0.028	0.540	10.506	18.558	0.003	62.090	1.685	0.237
9.900	6.710	-0.144	0.028	0.540	10.518	18.572	0.003	63.363	1.715	0.242
10.000	6.672	-0.155	0.028	0.540	10.535	18.585	0.003	64.650	1.746	0.248

Appendix D.2 Power Required vs. Power Available

Speed vs. P_A, P_R

Speed	Power Required	Power Available
1.00	52.20	8.87
1.10	47.46	9.74
1.20	43.51	10.61
1.30	40.17	11.48
1.40	37.31	12.34
1.50	34.83	13.20
1.60	32.66	14.05
1.70	30.75	14.91
1.80	29.05	15.76
1.90	27.53	16.60
2.00	26.17	17.45
2.10	24.94	18.29
2.20	23.82	19.12
2.30	22.81	19.95
2.40	21.88	20.78
2.50	21.02	21.61
2.60	20.24	22.43
2.70	19.52	23.25
2.80	18.85	24.06
2.90	18.23	24.88
3.00	17.65	25.68
3.10	17.12	26.48
3.20	16.62	27.27
3.30	16.15	28.05

3.40	15.72	28.83
3.50	15.32	29.61
3.60	14.94	30.38
3.70	14.58	31.14
3.80	14.25	31.90
3.90	13.94	32.66
4.00	13.65	33.41
4.10	13.38	34.16
4.20	13.12	34.90
4.30	12.89	35.65
4.40	12.66	36.39
4.50	12.46	37.12
4.60	12.26	37.86
4.70	12.08	38.59
4.80	11.91	39.32
4.90	11.76	40.04
5.00	11.61	40.75
5.10	11.48	41.45
5.20	11.36	42.14
5.30	11.25	42.82
5.40	11.15	43.49
5.50	11.06	44.16
5.60	10.97	44.83
5.70	10.90	45.49
5.80	10.84	46.14
5.90	10.78	46.80
6.00	10.73	47.45
6.10	10.69	48.10
6.20	10.66	48.74
6.30	10.64	49.38
6.40	10.62	50.01
6.50	10.61	50.63
6.60	10.61	51.24
6.70	10.62	51.84
6.80	10.63	52.44

6.90	10.66	53.03
7.00	10.68	53.61
7.10	10.72	54.19
7.20	10.76	54.76
7.30	10.81	55.32
7.40	10.87	55.87
7.50	10.93	56.41
7.60	11.00	56.94
7.70	11.08	57.46
7.80	11.16	57.98
7.90	11.25	58.49
8.00	11.34	58.99
8.10	11.45	59.49
8.20	11.55	59.97
8.30	11.67	60.45
8.40	11.79	60.91
8.50	11.92	61.36
8.60	12.06	61.79
8.70	12.20	62.20
8.80	12.35	62.60
8.90	12.50	62.99
9.00	12.66	63.37
9.10	12.83	63.74
9.20	13.00	64.09
9.30	13.18	64.44
9.40	13.37	64.78
9.50	13.56	65.12
9.60	13.76	65.46
9.70	13.97	65.79
9.80	14.19	66.12
9.90	14.41	66.43
10.00	14.63	66.72
10.10	14.87	66.98
10.20	15.11	67.23
10.30	15.35	67.47

10.40	15.61	67.69
10.50	15.87	67.89
10.60	16.13	68.08
10.70	16.41	68.26
10.80	16.69	68.43
10.90	16.98	68.58
11.00	17.27	68.73
11.10	17.58	68.87
11.20	17.88	68.99
11.30	18.20	69.10
11.40	18.52	69.19
11.50	18.85	69.26
11.60	19.19	69.32
11.70	19.54	69.29
11.80	19.89	69.18
11.90	20.25	69.01
12.00	20.62	68.81
12.10	20.99	68.63
12.20	21.37	68.48
12.30	21.76	68.40
12.40	22.16	68.46
12.50	22.56	68.70
12.60	22.97	69.20
12.70	23.39	69.58
12.80	23.82	69.75
12.90	24.25	69.78
13.00	24.70	69.72
13.10	25.15	69.61
13.20	25.60	69.47
13.30	26.07	69.34
13.40	26.54	69.26
13.50	27.03	69.25
13.60	27.52	69.28
13.70	28.01	69.33
13.80	28.52	69.35

13.90	29.03	69.33
14.00	29.56	69.23
14.10	30.09	69.02
14.20	30.63	68.58
14.30	31.18	68.31
14.40	31.73	68.15
14.50	32.30	68.07
14.60	32.87	68.04
14.70	33.45	68.05
14.80	34.04	68.06
14.90	34.64	68.07
15.00	35.25	68.03
15.10	35.87	67.92
15.20	36.49	67.70
15.30	37.12	67.37
15.40	37.77	67.14
15.50	38.42	66.99
15.60	39.08	66.89
15.70	39.75	66.81
15.80	40.43	66.74
15.90	41.12	66.67
16.00	41.82	66.56
16.10	42.52	66.44
16.20	43.24	66.32
16.30	43.97	66.20
16.40	44.70	66.07
16.50	45.45	65.94
16.60	46.20	65.80
16.70	46.97	65.65
16.80	47.74	65.49
16.90	48.52	65.32
17.00	49.32	65.15
17.10	50.12	64.95
17.20	50.93	64.74
17.30	51.75	64.52

17.40	52.59	64.29
17.50	53.43	64.05
17.60	54.28	63.81
17.70	55.15	63.57
17.80	56.02	63.33
17.90	56.90	63.09
18.00	57.80	62.87
18.10	58.70	62.65
18.20	59.61	62.43
18.30	60.54	62.21
18.40	61.48	61.98
18.50	62.42	61.75
18.60	63.38	61.49
18.70	64.34	61.22
18.80	65.32	60.93
18.90	66.31	60.62
19.00	67.31	60.30
19.10	68.32	59.96
19.20	69.34	59.62
19.30	70.38	59.26
19.40	71.42	58.89
19.50	72.47	58.52
19.60	73.54	58.14
19.70	74.62	57.75
19.80	75.70	57.36
19.90	76.80	56.97
20.00	77.91	56.58

References

Introduction Citations

[A1] P.Grant (2023). AER406: intro_extended.

[A2] *Weight and Balance Handbook*, U.S. Department of Transportation Federal Aviation Administration, 2016. https://www.faa.gov/regulations_policies/handbooks_manuals/aviation/media/faa-h-8083-1.pdf

[A3] P.Grant (2023). AER406: Important Resources: "Equip", slide 16.

[A4] E. Cordier, "Flutter is an unstable oscillation which can lead to destruction.," *Flight Mechanics and aerodynamics*. [Online]. Available: http://aviation.cours-de-math.eu/ATPL-081-POF/flutter.php

[A5] J. Shipe, "Aircraft antenna installations," *Cessna Owner Organization*, 05-Feb-2020. [Online]. Available: https://cessnaowner.org/aircraft-antenna-installations/

[A6] "Stability," *SKYbrary Aviation Safety*. [Online]. Available: https://www.skybrary.aero/articles/stability

Performance Citations

[P1] H. Liu (2021). AER302: Steady Flight Performance

[P2] H. Liu (2021). AER302: Accelerated Flight Performance

Stability Citations

[E1] "Participation handbook - akamodell-muenchen.de." [Online]. Available: https://akamodell-muenchen.de/wp-content/uploads/2021/03/regulations_acc_2022_munich_v01_11.pd

[E2] R.M.Martinez, *Design and Analysis of the Control and Stability of a Blended Wing Body Aircraft,"* Royal Institute of Technology, 2014.

[E3] D.P.Raymer, *Aircraft Design: A Conceptual Approach*, 2nd ed.Washington: AIAA, 1992, pp. 124.

[E4] P.Grant (2023). AER406: Equip.